REPORT DOCUMENTATION PAGE

Form Approved OMB No. 0704-0188

1. REPORT DATE *(DD-MM-YYYY)*	2. REPORT TYPE	3. DATES COVERED *(From – To)*
18-07-2006	Final Report	1 May 2005 - 01-May-06

4. TITLE AND SUBTITLE

Microdischarge Sources of O_2(singlet Delta)

5a. CONTRACT NUMBER
FA8655-05-1-3038

5b. GRANT NUMBER

5c. PROGRAM ELEMENT NUMBER

6. AUTHOR(S)

Dr. Leanne C Pitchford

5d. PROJECT NUMBER

5d. TASK NUMBER

5e. WORK UNIT NUMBER

7. PERFORMING ORGANIZATION NAME(S) AND ADDRESS(ES)
CPAT
118 Route de Narbonne
Toulouse 31062
France

8. PERFORMING ORGANIZATION REPORT NUMBER
N/A

9. SPONSORING/MONITORING AGENCY NAME(S) AND ADDRESS(ES)

EOARD
PSC 821 BOX 14
FPO AE 09421-0014

10. SPONSOR/MONITOR'S ACRONYM(S)

11. SPONSOR/MONITOR'S REPORT NUMBER(S)
Grant 05-3038

12. DISTRIBUTION/AVAILABILITY STATEMENT

Approved for public release; distribution is unlimited.

13. SUPPLEMENTARY NOTES

14. ABSTRACT: The focus was to to obtain yield measurements in DC microdischarges, but there will also be an important modeling component conducted in parallel with the experiments. The existing MHCD model was developed for rare gases, and this will be extended to include a description of the O2 kinetics, based on previously published work. A particularly important parameter is the gas temperature, and the gas heating source term in the model also needs to be extended to include V-T (vibrational to translation) energy exchange - ion heating in the sheath (expected to be the dominant component) is included in our present model). We originally proposed measuring the O2(1D) yield using IR absorption spectroscopy, and we still feel that it will eventually be necessary to develop this or another or the more traditional spectroscopic methods (eg CARS or UV absorption). However, during the proof-of-principle phase of this project, we propose using an isothermal calorimeter as has been developed previously for measurements of O2(1D) yields by several groups7,8. We have been in contact with Dr. Ikonnikov, and he has kindly provided us with additional information on the set-up of Lodin et al7. This calorimetric technique is, in our opinion, the best way to obtain a quick, inexpensive, and accurate estimate of the O2(1D) yield in a single microdischarge operating in a DC mode. The experimental set-up is simple - a nickel coil is positioned in the gas flow on the downstream side of the microdischarge and the chemical energy in the gas flow is detected as a change in the external power required to maintain the coil at a constant temperature (eg 150°C). This power is reduced when O2(1D) is deactivated at the coil surface. The Russian group7 used a self-balancing bridge circuit to maintain the constant temperature and they calibrated their system by measuring the O2(1D) emission signal before and after the detector. They determined that between 70 and 90% of the O2(1D) reacted with the nickel coil for their experimental conditions. Based on the results of Lodin et al, we estimate that O2(1D) yields as low as 5% can be measured with this technique. In its simplest implementation, the method is limited to volume integrated measurements of O2(1D) yields and for DC discharges.

15. SUBJECT TERMS
EOARD, Plasma Physics and Chemistry, Gas Discharge, Electric lasers

16. SECURITY CLASSIFICATION OF:

a. REPORT	b. ABSTRACT	c. THIS PAGE
UNCLAS	UNCLAS	UNCLAS

17. LIMITATION OF ABSTRACT
UL

18, NUMBER OF PAGES
54

19a. NAME OF RESPONSIBLE PERSON
DONALD J SMITH

19b. TELEPHONE NUMBER *(Include area code)*
+44 (0)20 7514 4953

Final report : Option 1 of the project entitled

Microdischarge sources of O$_2$($^1\Delta$)

Project partners :

Leanne Pitchford and Jean-Pierre Boeuf
Centre de Physique des Plasmas et Applications de Toulouse (CPAT)
University Paul Sabatier and CNRS, Toulouse, France

Vincent Puech
Laboratoire de Physique des Gaz et des Plasmas (LPGP)
Université Paris-Sud and CNRS, Paris, France

Antoine Rousseau
Laboratoire de Physique et Technologie des Plasmas (LPTP)
Ecole Polytechnique and CNRS, Palaiseau, France

Report prepared by:

Leanne Pitchford
e-mail : pitchford@cpat.ups-tlse.fr
tel : +33 (0) 5 61 55 64 81

Vincent Puech
e-mail : vincent.puech@pgp.u-psud.fr
tel : +33 (0) 01 69 15 78 77

Table of contents

List of figures

Summary

This report describes work performed as an Option 1 follow-up to our previous report from December 2005[1]. In the December report, we described in detail the operation of microdischarges in pure argon in two and three electrode configurations. These first experiments and model calculations were carried out in pure argon in order to develop techniques and expertise needed for subsequent experiments in oxygen containing mixtures. The results described in this report are all for oxygen containing mixtures.

In the two-electrode configuration, we have a simple electrode/dielectric/electrode sandwich through which a central hole has been drilled. The hole diameter and the dielectric thickness are both on the order of 200 μm. Schoenbach and his colleagues developed this concept [2] and showed that stable, non-thermal, high-pressure discharges can be generated and maintained in this configuration. *This is called a MicroHollow Cathode Discharge or MHCD.*

More interesting for the generation of $O_2(^1\Delta)$ *is the configuration called Micro Cathode Sustained Discharge[3] (MCSD).* This is a three-electrode configuration in which the MHCD is used as a plasma cathode for a discharge with a third electrode, an anode, placed some 5 to 10 mm away, as shown schematically in the figure below. Our report from December 2005 described in detail the initiation of the MCSD discharge in this 3-electrode configuration.

Both the MHCD and the MCSD configuration are illustrated schematically in fig. S-1.
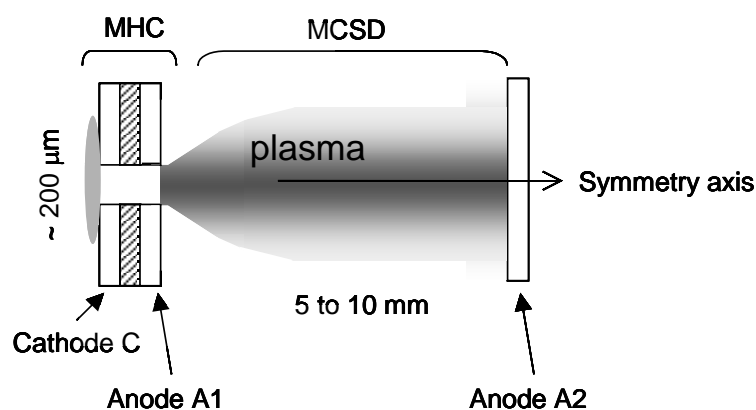
Fig. S-1. Schematic of the plasma created in a Micro Cathode Sustained Discharge – MCSD. This is a discharge sustained by a Micro Hollow Cathode (MHC) acting as a plasma cathode. Drawing not to scale.

The plasma in the MCSD volume is remarkable for its stability at high pressure, and this property is directly related to the stability of the cathode region – the MHCD. We showed previously that the electric field in the MCSD region is relatively low and typical of a positive-column type plasma[1]. This combination of low field and stable, high-pressure plasma region is especially interesting for the application of interest here - the generation of high yields of $O_2(^1\Delta)$.

In this report, we present an experimental and modeling characterization of the plasma in the MCSD region in oxygen containing mixtures. These are first results, and given the time constraints, we have not had the time to understand fully the reasons for all the trends we observe. Our purpose during these last few months has been to show that high yields of $O_2(^1\Delta)$ can indeed be generated in these discharge configurations, and we have been successful in achieving showing this.

We have measured $O_2(^1\Delta)$ yields of up to 7.6% in mixtures of Ar/O_2 in a measurement cell downstream from the reactor. The yields measured downstream can be considered as a lower limit to the yields obtained in the reactor. Our original plan was to use a calorimeter system as a diagnostic of the $O_2(^1\Delta)$. The calorimeter was constructed, but has yielded null results after much effort. We therefore spent the last few months refining the use of emission spectroscopy as a diagnostic of the $O_2(^1\Delta)$. While the yields inferred from measurements of the 1.27 micron radiation resulting from radiative deexcitation of the $O_2(^1\Delta)$ are extremely interesting, it is important to emphasize that more diagnostics and modeling are needed to confirm these figures.

The highlights of our results in oxygen reported here are :
- The experimental system is up and running in oxygen containing plasmas, and it is equipped with several different electrical and optical diagnostics.
- Generation of stable, high-pressure non-thermal plasmas in oxygen containing mixtures is possible in microdischarge configurations. Results have been obtained for discharges in Ar/O_2 mixtures with total pressures up to 130 torr. Higher pressure operation is possible – we are limited at the moment simply by our pressure gauges.
- We have measured properties of the plasma in the interesting, MCSD region : the inferred electric field is relatively low and dependent on the gas mixture as well as the gas flow rate.
- Absolute number densities of O atoms, [O], in pure oxygen discharges and of [O_3] have in Ar/O2 mixtures been measured as well as their spatial distributions.
- The gas temperature in the MCSD region has been measured, and it is low (400 K or less) over the range of conditions studied.
- The calorimeter diagnostic for the $O_2(^1\Delta)$ concentrations has so far yielded null results. Therefore, $O_2(^1\Delta)$ yields were measured using emission spectroscopy. This diagnostic is difficult because of weak signals and so far we have been able to measure these yields only in Ar/O_2 mixtures and only at points downstream from the reactor. *$O_2(^1\Delta)$ yields of up to 7.6% have been observed 23 cm downstream from the reactor.*
- Parallel operation of four MCSDs has been demonstrated in Ar/O_2 mixtures, confirming that scale-up is possible.
- A two-dimensional model of the MCSD has been developed which includes the details of the Ar/O_2 plasma chemistry and yields a self-consistent electric field distribution and species number densities.
- The calculated electric field is in reasonable agreement with the experiment. The calculated $O_2(^1\Delta)$ yields are on the order of those measured.

In summary, microdischarges operating in an MCSD mode are a promising source of $O_2(^1\Delta)$. In these first experiments reported here, we have shown that it is possible to
- *generate* high yields of $O_2(^1\Delta)$
- *transport* it 10's of cm downstream, and
- *scale-up* the discharge volume by operating multiple discharge in parallel.

7

While these results are very promising, the $O_2(^1\Delta)$ yield measurements in particular need to be cross-checked with other more sophisticated diagnostic techniques.

In Section X of this report, we outline some future directions.

I. Experimental set-up

A photograph of the experimental set-up at Laboratoire de Physique des Gaz et des Plasmas (LPGP) is shown in fig. I-1.
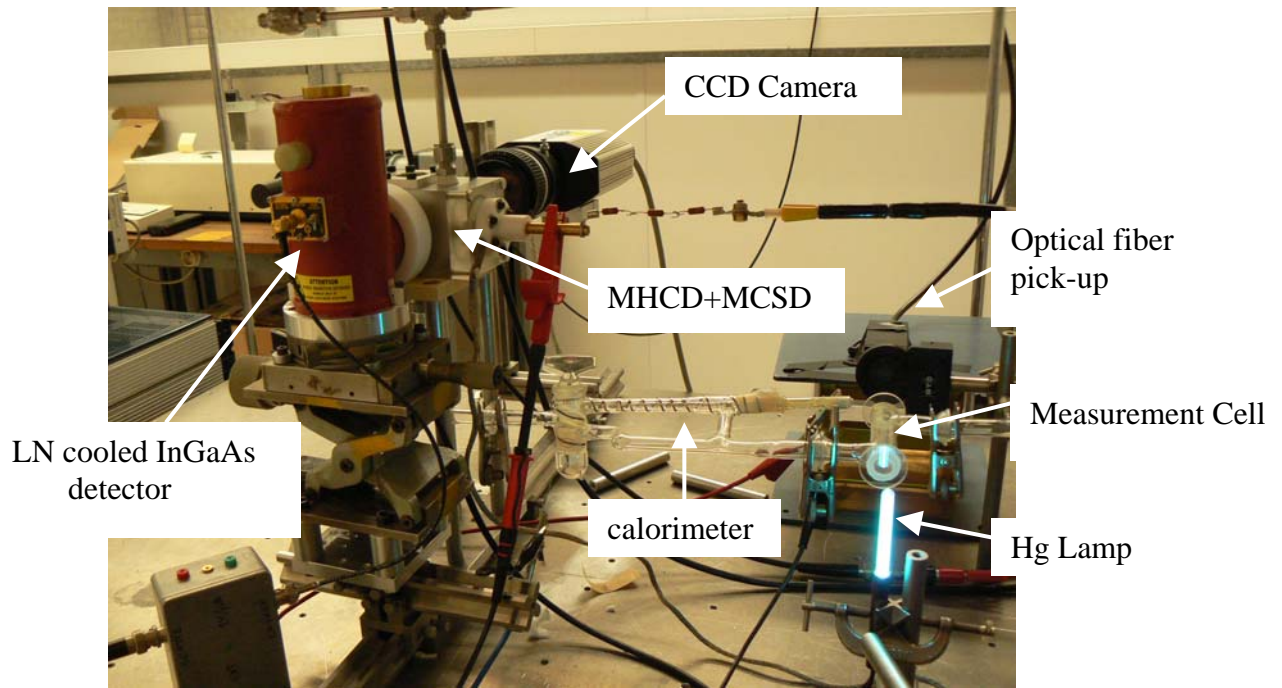
Figure I-1: Photograph of the experimental set-up and diagnostics

A stainless steel cell – the "reactor" – contains the MHCD sandwich and MCSD, and it is shown in the photograph in figure I-2. The MHCD itself consists of two molybdenum electrodes of thickness 100 μm separated by a dielectric (mica) plate. A cylindrical hole is drilled through the center of the sandwich, and the diameter of the hole is typically about the same as the dielectric thickness. We used two geometries, one with a MHCD hole diameter of 200 μm and dielectric thickness 150 μm and a second geometry with a hole diameter of 400 μm and dielectric thickness of 450 μm. Unless otherwise stated, all results shown here are for the larger geometry. No notable differences were observed in the MCSD plasma for the two different hole diameters. The significant advantage of the larger hole diameter is longer lifetime. For the 400 μm diameter MHCD, it is possible to use the same experimental device for over a week of continuous experiments with no measurable change in the discharge properties, whereas the 200 μm diameter MHCDs had to be replaced every few days.

A negative voltage is applied to the cathode, C, through a ballast resistor of 1 MΩ. The second electrode, the anode A1, is grounded through in intermediate resistor of 100 Ω. This MHCD serves as a plasma cathode for a discharge with larger volume between the MHCD and a third electrode (an anode - A2), cylindrical and with a diameter of 25 mm and place 8 mm from the MHCD. The electrode A2 is powered through a 660 kΩ resistor. Figures I-3 and I-4 show respectively photos of the plasma along the back surface of the cathode when the MHCD is operating in a self-pulsing mode in argon and the MCSD - the discharge sustained between the MHCD and anode A2 - in oxygen.

The reactor volume is much larger than the volume exposed to the discharge in order to provide optical access. The design is such as to minimize the excess volume, while allowing room for coupling to diagnostics and in particular for the imaging, optical emission and absorption spectroscopy, and laser induced fluorescence (LIF). The gas inlet is 15 mm directly over the center of the MCSD and the evacuation is opposite and 15 mm underneath. After passing through the discharge chamber, the gas flow is directed towards the calorimeter and a measurement cell which is shown in the photo in fig. I-1. This cell is cylindrical with flat end faces of quartz; it has a length of 82 mm and a diameter of 14 mm.
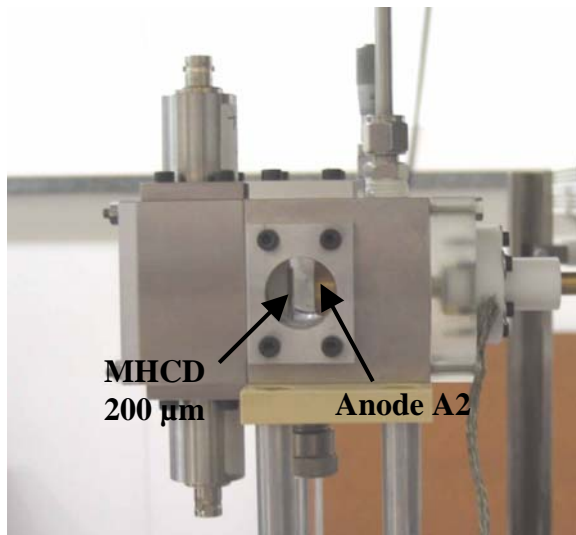
Figure I-2: View of the reactor
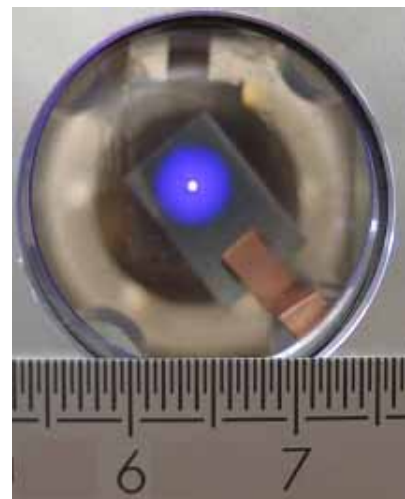
Figure I-3: View of the back face of the cathode showing a discharge in argon spreading along the cathode surface for a MHCD discharge operating in a self-pulsing mode.
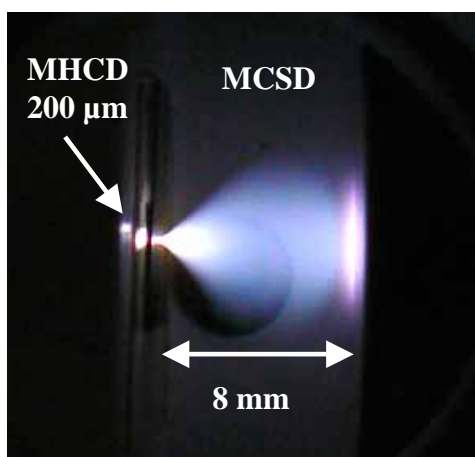
Figure I-4: Photograph of a MCSD operating at 1 mA in 50 torr pure oxygen.

After evacuating the system with primary pumping, there is a continuous gas flow through the reactor. For the results reported here, we used flow rates between 5 and 40 sccm for the oxygen with the rare gas flow rates between 60 and 430 sccm. The flow rates are measured using a flowmeter (Brooks, model 1355) and the pressure in the reactor is measured using a Baratron with a range from 0 to 133 torr. The practical lower limit for the pressure is about 25 torr, below which breakdown occurs between the cathode and the cell walls.

Electrical and optical diagnostics are used to study the operation of both the MHCD and the MCSD discharges. For all experimental conditions, we measure the voltages and currents at the MHCD and at the MHCD with high voltage probes and a numerical oscilloscope (350 MHz Lecroy LT264). Optical diagnostics used to study the plasma in the MCSD volume are :
- 12 bit CCD camera imaging, allowing us to record the spatial distribution of radiation from MCSD as a function of operating conditions
- emission spectroscopy in the interval 760-780 nm, which provides information about the intensity of the atmospheric band in molecular oxygen (transition O_2 ($b^1\Sigma_g^+$, v = 0) $\rightarrow O_2$ ($X^3\Sigma_g^-$, v = 0) as well as the emission from atomic oxygen in the O*(5p), level.
- absorption measurements at 253 nm for measurements of [O_3]
- laser induced fluorescence (LIF) measurements to determine the [O]
- measurements of the intensity of the 1.27µm radiation resulting from radiative deexcitation of $O_2(a^1\Delta_g)$ to infer the yield.

Figure I-5 shows the measurement panels : these are from left to right oscillograms, emission spectra from the plasma in the wavelength interval from 760 to 780 nm, and CCD camera imagines of the plasma in the MCSD region.
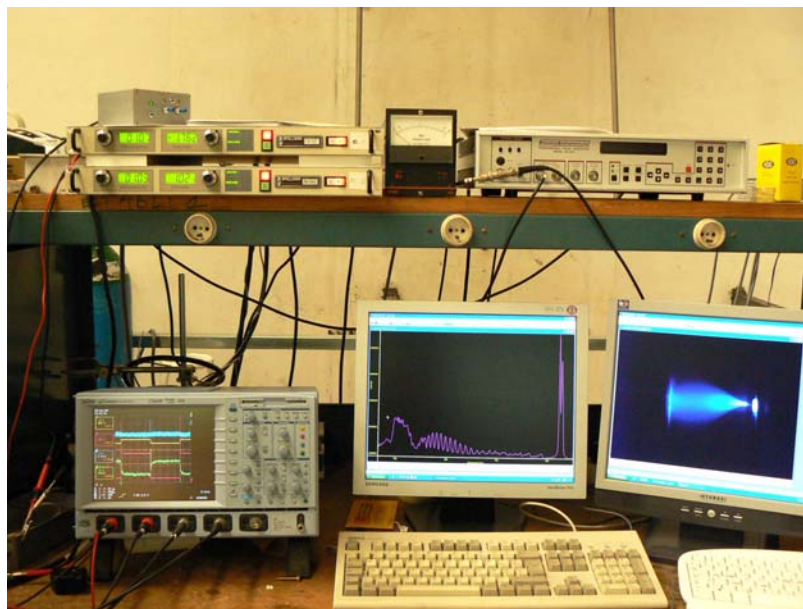
Figure I-5: Photograph of measurement panels

II- Electrical characteristics of the MCSD

The molecular states $O_2(a^1\Delta)$ and $O_2(b^1\Sigma)$ are produced exclusively in the relatively low electric field volume of the MCSD and not in the high-field regions in the MHCD, as we will see below. We are therefore mainly interested in the electrical characteristics of the MCSD – the voltage on anode A2, V_{A2}, and the current collected by anode A2, I_{A2}, for a given current through the MHCD, I_C. For the results reported below, we concentrate on pure oxygen and mixtures of argon or helium with oxygen, with total pressures between 25 and 130 torr and for MHCD currents between 0.1 and 2 mA. The MHCD alone operates in a self-pulsing mode for these conditions in mixtures with oxygen but when the MCSD is initiated, the MHCD switches immediately to a DC mode – the self-pulsing disappears. The reasons for this are not fully understood at this time. The self-pulsing model is described in detail in the articles submitted for publication by Auber et al[4] and discussion following fig. VII-2.

Figure II-1a shows the voltage-current, V-I, characteristic in the MCSD for 50 torr oxygen and for a gas flow rate of 40 sccm. Figure II-1b shows the same results in a mixture of Ar/O$_2$ with 10 % de O$_2$ for a total pressure of 50 torr with a total flow rate of 239 sccm. Results are shown for two different values of the current from the MHCD, 0.5 and 1 mA. Starting with only the MHCD operating, initiation of a plasma in the MCSD region requires application of a high voltage. Once initiated, the voltage required to sustain a plasma in this volume is much less than the initiation voltage. The current carried by the MCSD depends on the voltage V_{A2}, and an increase in the current in the MCSD leads to a slow decrease in V_{A2} (negative characteristic) up to the point where the $I_C = I_{A2}$ where all the current is collected by anode A2 and none by anode A1. The point $I_C = I_{A2}$ is indicated by the arrows in figs. II-1. Increasing the current I_{A2} past this point requires an increasing voltage because an electron current must be drawn from A1. We find that the point $I_C = I_{A2}$ represents a limit in the sense that if we increase the current further, the MCSD becomes self-sustaining. It is then to turn off the MHCD. The MCSD discharge continues to be stable and anchored to the MHCD hole region.
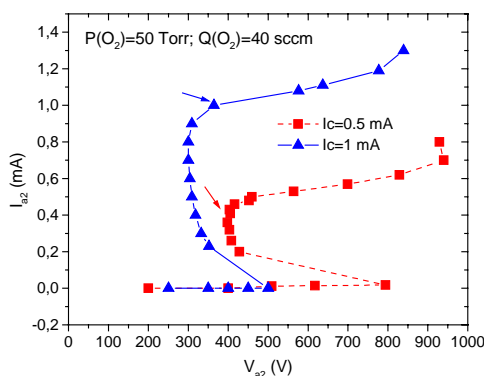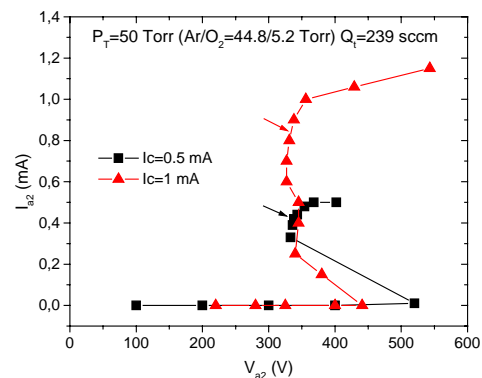
a)   b)

Fig. II-1 Voltage-current characteristic of the MCSD for two values of the current flowing in the MHCD, 0.5 and 1 mA. (a) 50 torr oxygen and (b) 50 torr Ar/O$_2$ with 10% O$_2$.

A plot of the MCSD voltage, V_{A2}, as a function of current for the operating point $I_{A2}=I_C$ is shown in fig. II-3 for an argon/oxygen mixture at 70 torr with 6% oxygen and a gas flow rate, Q, of 227 sccm. There is more work to be done to understand the reasons for this negative characteristic.
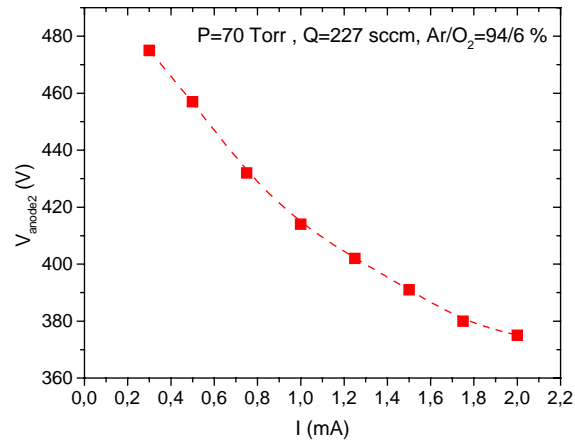
Fig. II-2. Voltage-current characteristic of the MCSD for points where $I_C = I_{A2}$ in an Ar/O$_2$ mixture with 5.9% O$_2$ at a total pressure of 70 torr and gas flow rate of 227 sccm.

In our previous report[1] we presented results showing that the voltage required to maintain the MCSD at the point $I_{A2} = I_C$ increases linearly with distance between anodes A1 and A2 in pure argon. The point $I_{A2} = I_C$ is significant in that this is the point where $I_{A1} = 0$ and there should therefore be no sheath (no voltage drop) surrounding this electrode. The observation that V_{A2} depends linearly on distance for $I_{A2} = I_C$ leads to the conclusion that the plasma in the MCSD region is similar to a positive column of a classical glow discharge whose role is simply to close the circuit between the cathode regions and the anode. In a positive column, the electric field is constant, and we interpreted the measured linear slope as an electric field of magnitude E. All experimental results and model calculations to date continue to support this conclusion.

The reduced electric field – E/p or E/N, the ratio of the field strength to the gas pressure, p, or neutral density, N – is a more useful parameter for describing the plasma because the electron mean energy is a function of this parameter. In the experimental system in Orsay, the distance between anodes A1 and A2 is fixed at 0.8 cm, but measurements were made as a function of pressure in order to estimate E/N in the MCSD plasma. Shown in fig. II-3 are values of V_{A2} at the point $I_{A2} = I_C$. These are shown as a function of gas pressure in Ar/O$_2$ mixtures with 5.9% oxygen and parametrically as a function of gas flow rate, Q. For Q constant, the voltage V_{A2} increases linearly with pressure, and the slope of the line V_{A2} vs p is proportional to E/N. Values of E/N are reported in units of Townsend (1 Td = 10^{-17} V cm^2) which is a standard unit for reduced electric field, E/N (N is the gas density, related to the pressure p through the ideal gas law - we return to the issue of gas temperature below - at 300 K, 1 torr corresponds approximately to 3.5 10^{16} molecules cm^{-3}). The values of E/N determined from the data in fig. II-3 are 13.9 Td for a flow of 78 sccm and 21 Td for a higher flow rate of 455 sccm. We do not fully understand the dependence on gas flow. Possible reasons are that the plasma column is blown by the flow (see Section III) such that its length is greater for high gas flows or more simply that the plasma conductivity depends on the degree of excitation in the gas. The evacuation of excitation by the gas flow would increase the conductivity and hence the E/N needed to conduct the current through the MCSD. More work is needed to understand the role of gas flow in these results and in the other results shown below.
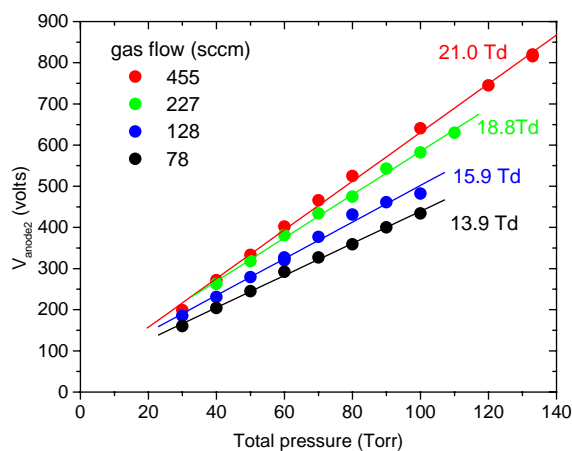
Figure II-3: MCSD voltage, V_{A2}, as a function of total gas pressure, for the operating point $I_{A2} = I_C = 0.5$ mA in Ar/O$_2$ with 5.9 % O$_2$ and for 4 different flow rates as indicated.

It is well known that low values of E/N favor excitation of $O_2(^1\Delta)$ over other inelastic channels in oxygen containing mixtures. In pure O_2 with no internal excitation, the optimum E/N is about 10 Td, at which value almost 50% of the electrical energy is deposited in excitation of $O_2(^1\Delta)$. As we showed in fig. 19 of our report in December 2005, the optimum E/N shifts to lower values in mixtures with argon or helium, but the fractional energy going into excitation of the $O_2(^1\Delta)$ is still significant at 10-15 Td. Therefore, the relatively low values of E/N estimated from the slopes in fig. II-3 is encouraging in the context of generation of high yields of $O_2(^1\Delta)$.

In contrast to the clear dependence of the electrical characteristics of the MCSD on gas flow rate, very little influence of the gas flow rate is observed in the measured V-I characteristics of the MHCD itself. This is shown in fig. II-4 for Ar/O_2 mixtures with 5 torr and 5.9% O_2.
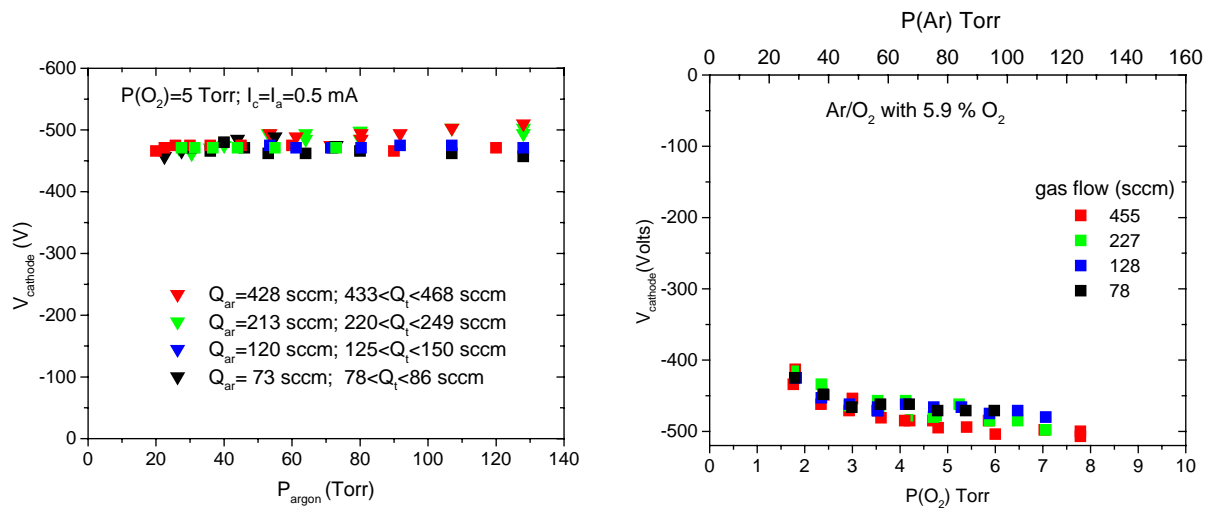
Figure II-4: MHCD voltage, V_C, as a function of total gas pressure for $I_{A2} = I_C = 0.5$ mA and for 4 different values of the gas flow rate, as in figs. II-4 and 5. The gas mixture is Ar/O_2 with 5 Torr (left panel) or 5.9% O_2 (right panel).

Replacing argon by helium, we find a slight increase in the MHCD voltage and a notable decrease in the MCSD voltage for a constant gas flow rate of about 430 sccm. This is shown in fig. II-5 where we have plotted the MHCD voltage as a function of partial pressure of oxygen for a total pressure of 112 torr and for $I_C = 0.5$ mA.
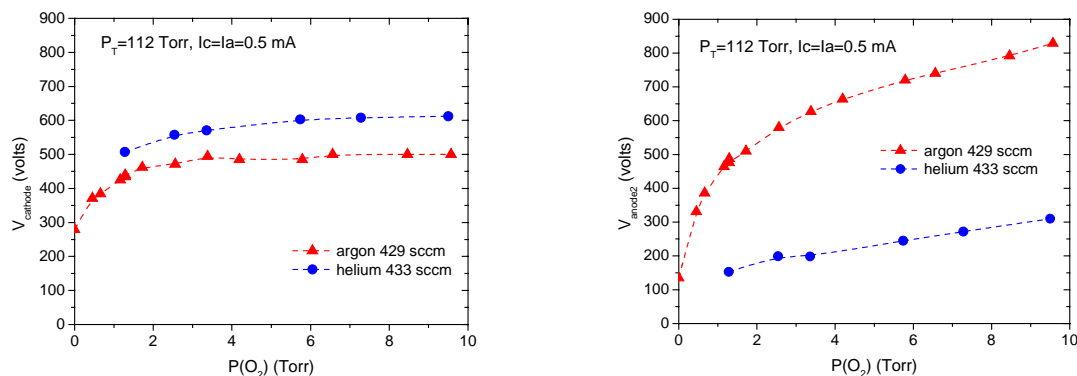
Fig. II-5. Comparison of the electrical characteristics of discharges in oxygen with argon or with helium. Left pane, MHCD; right panel, MCSD.

III-Visual appearance of the plasma in the MCSD region

In this section we show photographs of the emission from the plasma in the MCSD region. In contrast to the figures shown in the rest of this report, the MHCD is on the right and the anode A2 is on the left. Recall that the distance between the exit plane of the MHCD and the anode A2 is 8 mm and the diameter of anode A2 is 2.5 cm. The direction of the gas flow is from top to bottom and the same camera settings are used for each photo in a given figure.

Summary of observations :
 - In all cases, there is bright plasma zone near the exit of the MHCD. The plasma expands radially from the exit of the MHCD up to a certain point beyond which the diameter of the plasma column is approximately constant. There is a further radial expansion of the luminous region immediately in front of the surface of anode A2, which is almost entirely covered by a luminous layer.
- The column diameter is smaller in oxygen than in pure Ar, He or in rare gas/O_2 mixtures.
- The photographs confirm that the discharge is not constricted, even at the highest pressure of 133 torr, corresponding to a pd (pressure x distance) product of more than 100 torr cm. This is quite remarkable and illustrates the reason for the large and increasing interest in microdischarges for different applications. The plasma conditions (low gas temperature – see below - high plasma density, high degree of excitation/dissociation) are unlike those that can be achieved in other discharge devices.
- There is a noticeable effect of gas flow on the plasma profile in pure argon and in the Ar/O_2 mixtures. The plasma column appears to be blown downstream by the flow towards the downstream, and the effect is to increase the length of the conducting channel We have not observed any effect of gas flow in the other mixtures used (O_2, He and He/O_2).
- The images with gas flow are stationary and quite reproducible.
- As a function of current, the luminous region in discharges in pure oxygen at 90 torr becomes brighter and the diameter of the column decreases slightly, but the discharge does not collapse into an on-axis arc.
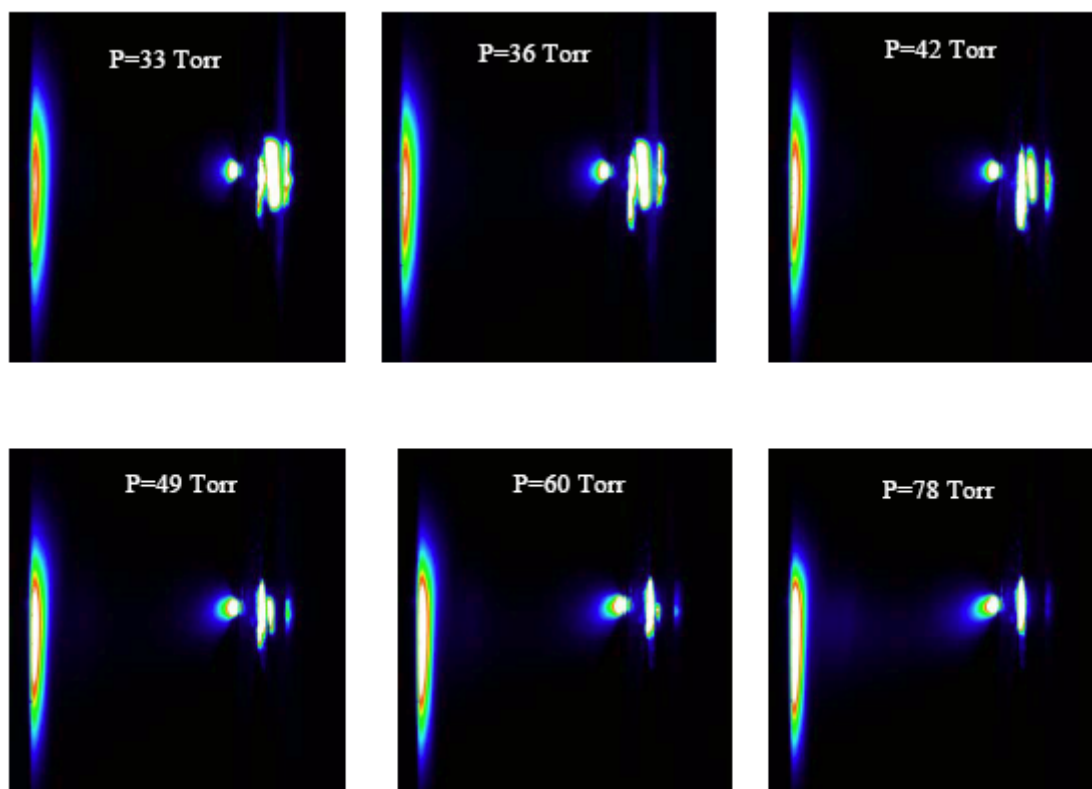
Figure III-1: Emission from the MCSD in Ar/O2 with 5 torr O_2 for different total pressures. $I_C = I_{A2} = 0.5$ mA. The gas flow rate is 78 sccm.
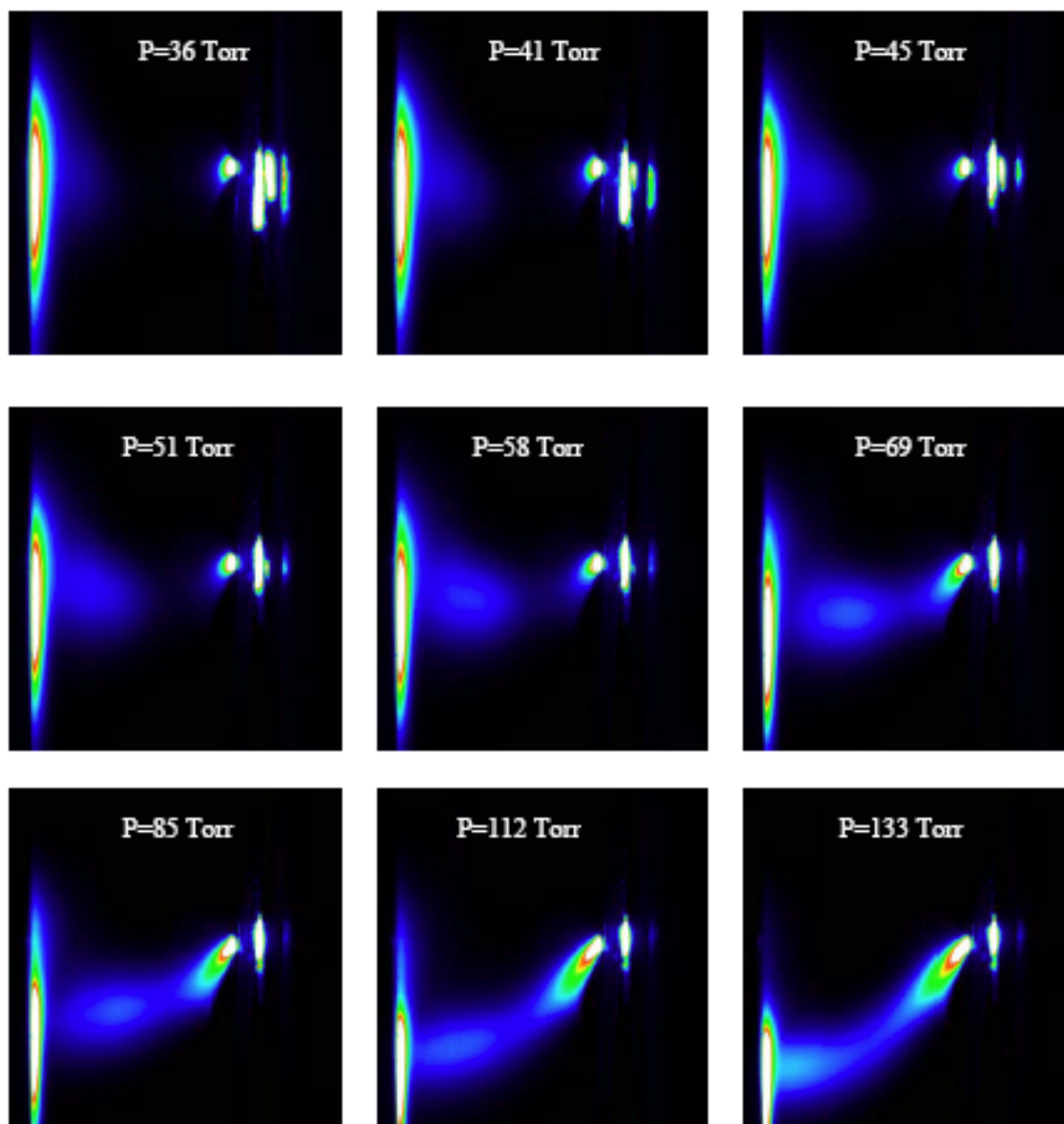
Figure III-2: Same as Fig. III-1 but for a gas flow rate of 214 sccm.

The emission from the plasma is stable and reproducible. The emission profile does not fluctuate in time and it is quite reproducible from one day to the next.
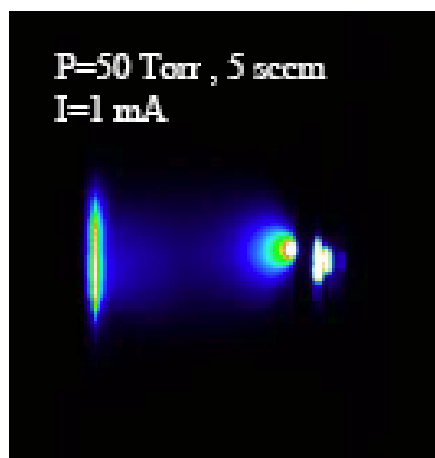
Figure III-3 : Emission from the MCSD in pure oxygen at 50 torr. Ic = IA2 = 1 mA.

There is no obvious influence of gas flow over the range 5 to 40 sccm.
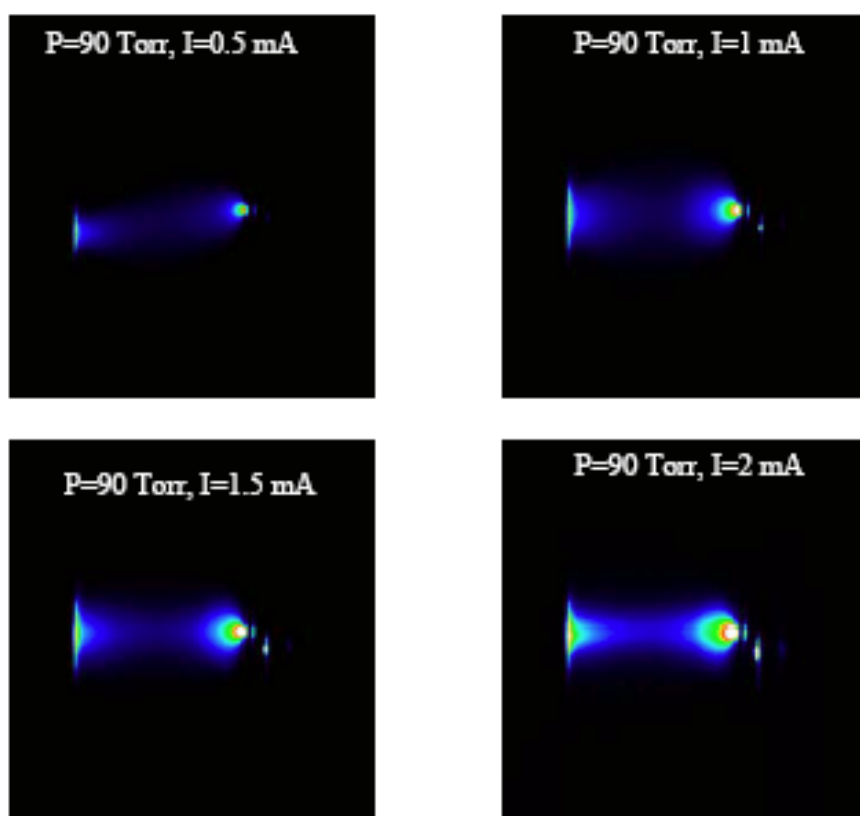
Figure III-4: Emission from the MCSD in 90 torr O_2 as a function of current ($I_C = I_{A2}$).
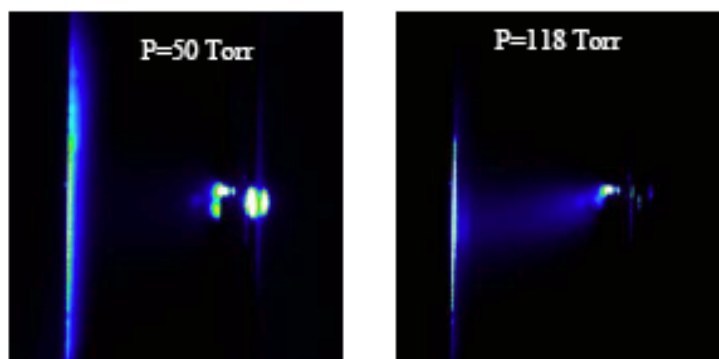
Figure III-5: Emission from the MCSD in pure Ar for a gas flow rate of 214 sccm and $I_C = I_{A2}$ = 0.5 mA.
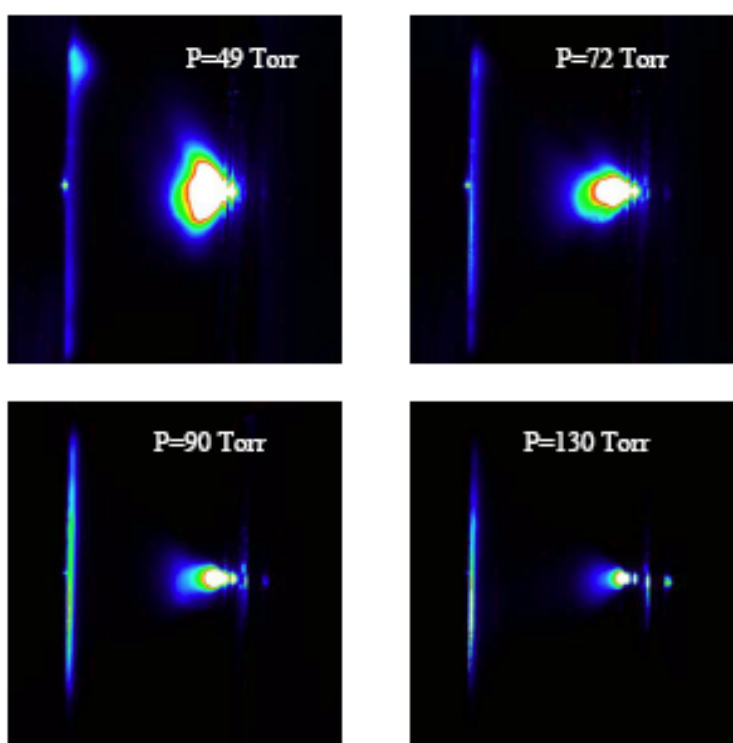
Figure III-6: Emission from the MCSD in pure He for a gas flow rate of 430 sccm. $I_C = I_{A2}$ = 0.5 mA.
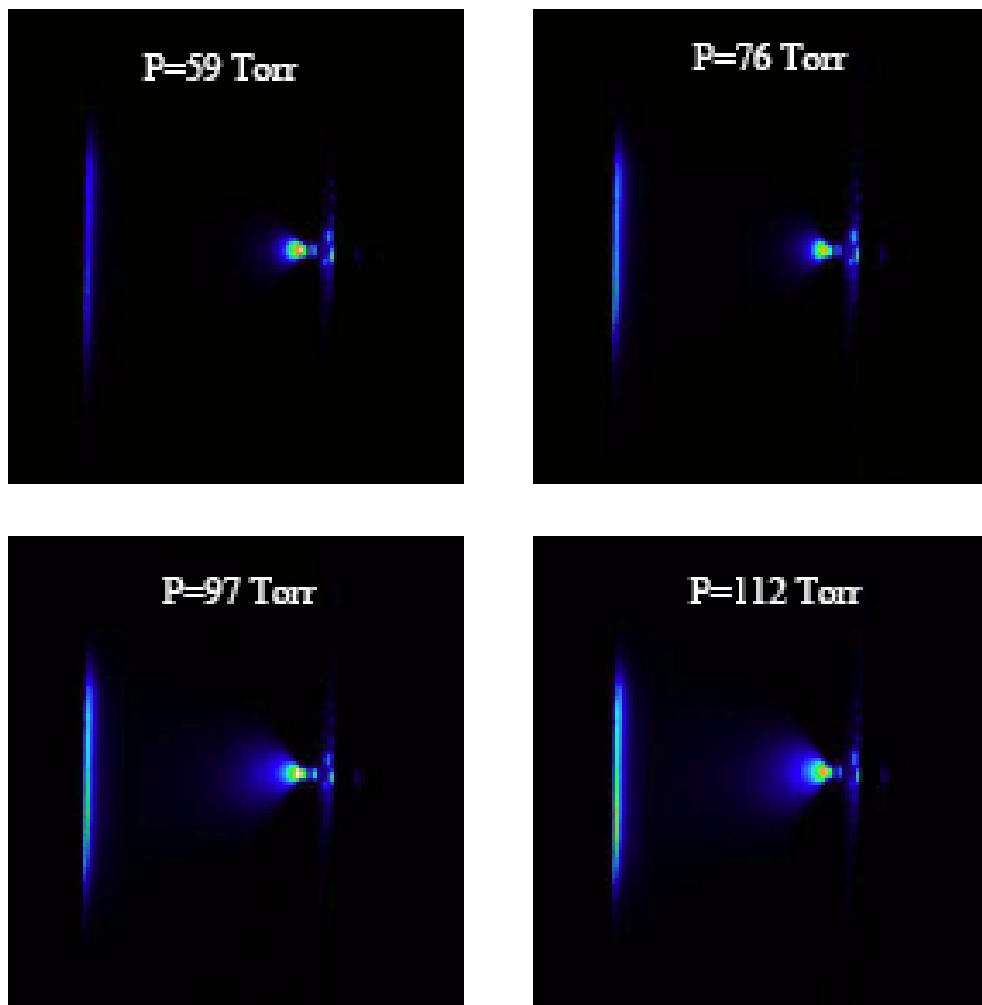
Figure III-7: Emission from the MCSD in He/O₂ with 5 torr He. $I_C = I_{A2} = 0.5$ mA and gas flow rate is 430 sccm.

The photo at 112 torr shows a perfectly centered plasma column, unperturbed by the gas flow, in contrast to the results shown in Ar/O₂ in fig. III-2 for a lower flow rate. We do not yet understand the influence of gas flow on the plasma in the MCSD.

IV-Spectroscopic studies in the 758 to 778 nm wavelength region

The first spectroscopic studies were carried out in the Laboratoire de Physique des Gaz et des Plasmas (LPGP) in Orsay. For these studies, a spectrometer equipped with a CCD camera with a spectral resolution of 0.1 nm was used. A typical spectrum over the wavelength range 758 to 778 nm is shown in fig. IV-1 where we can identify the molecular bands corresponding to rotational transitions of the infrared atmospheric band $O_2 (b^1\Sigma_g^+, v = 0) \rightarrow O_2 (X^3\Sigma_g^-, v = 0)$

and to an apparent doublet (actually an unresolved triplet) corresponding to radiation emitted by the 5p state of atomic oxygen.
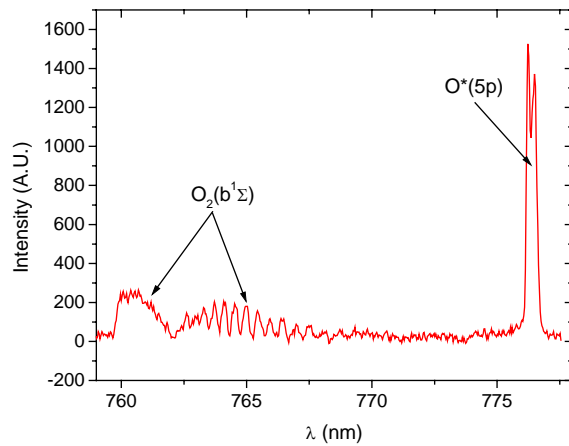
Figure IV-1: Low resolution spectrum of a discharge MHCD + MCSD in oxygen at 50 torr with a discharge current $I_C = I_{A2} = 1$ mA.

Emission from $O_2(^1\Sigma, v = 0)$ and O*(5p)

The MHCD operating alone is an intense source of emission of the atomic line at 777 nm, the intensity of which increases proportional to the discharge current as shown in fig. IV-2. Emission from the molecular atmospheric band is barely observed – it is at the detection limit – when the MHCD is operating alone (zero voltage on the MCSD).
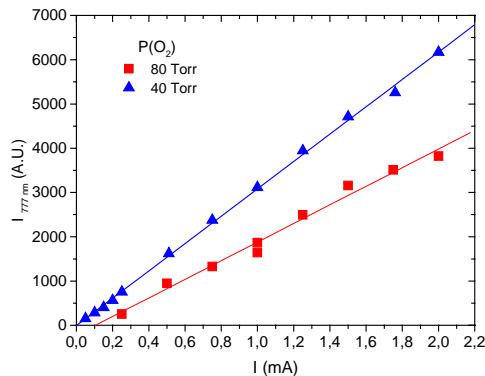
Figure IV-2: Intensity of the atomic line at 777 nm as a function of discharge current from the MHCD operating alone.

Now let us consider the spectra with both MHCD and MCSD powered. We looked at the spatial distribution of the emission from the atmospheric band with a resolution of 1.5 mm. For all discharge conditions studied, the molecular emission originating from the $O_2(b^1\Sigma_g^+)$ state is observed only in a localized region along the MCDS axis with an average diameter of about 5 mm along the 8 mm separation between the MHCD and the electrode A2. From this observation, we infer that the lifetime of this species is less than its diffusion time. Thus, emission from this band reflects the properties of the plasma near the discharge axis rather than an average of the gas properties over the reactor volume. An analysis of the atmospheric band can therefore be used to derive a rotational temperature of the $O_2(b^1\Sigma_g^+, v= 0)$ level as a function of position in the MCSD.

Line-of-sight intensities as a function of axial position for the 777 nm atomic emission and emission from the $O_2(b^1\Sigma_g^+, v= 0)$ level are shown in fig. IV-3. This data illustrates the very different behaviors of radiating levels : the [O*(5p)] decreases rapidly with increasing distance from the MHCD, becoming almost zero in the mid-plane before rising again in front

of the anode A2. In contrast, the $[O_2(b^1\Sigma_g^+, v = 0)]$ is much more homogeneous in the MCSD volume (but not in the *reactor* volume as discussed above).
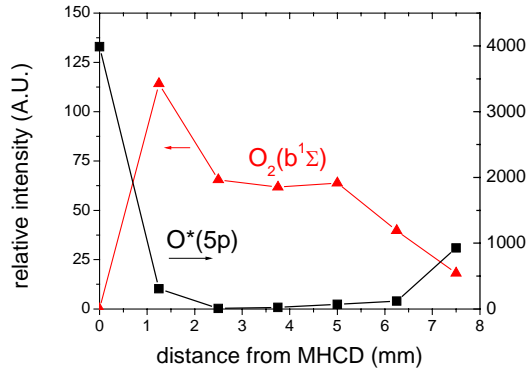
Figure IV-3: Axial distribution of intensities of radiation resulting from electronically excited molecules in the $O_2(b^1\Sigma_g^+, v = 0)$ state and from atoms in the 5p state.

Rotational temperature

As described, for example, by Touzeau et al in ref.5, an analysis of the distribution of the intensities of the individual rotational transitions in the atmospheric band yields the rotational temperature of the level O_2 ($b^1\Sigma_g^+$, v = 0). For the gas pressures considered here (p > 30 torr), it is reasonable to suppose that the rotational temperature is the same as the gas temperature.
    The intensity of a rotational line corresponding to a transition from an upper level J' to a lower level J'' depends on T and is given by ,

$$I_{J'}^{J''} = C. \ S_{J'}^{J''}.\exp(\frac{E_r}{k.T})$$

where C is a proportionality constant, $S_{J'}^{J''}$ is the Höln-London factor , E_r is the energy of the rotational level J. To first order, the rotational energy is given by $E_r = B_V .J.(J+1)$, where

B_V = 1.39138 cm^{-1} . A curve representing $\ln(\frac{I_{J'}^{J''}}{S_{J'}^{J''}})$ as a function of J.(J+1), a Boltzmann

plot, should be a straight line with a slope equal to - ($\frac{B_V}{k.T}$).

In order to determine the gas temperature in these microdischarges with a good precision, we solicited the involvement of Dr. Michel Touzeau who performed a series of experiments using the high-resolution (0.017 nm) resolution spectrometer available at the Laboratoire de Spectrométrie Physique in Grenoble. This high resolution allows to clearly distinguish the [P]P et [P]Q branches from each level J of the atmospheric band shown in fig. IV-4.
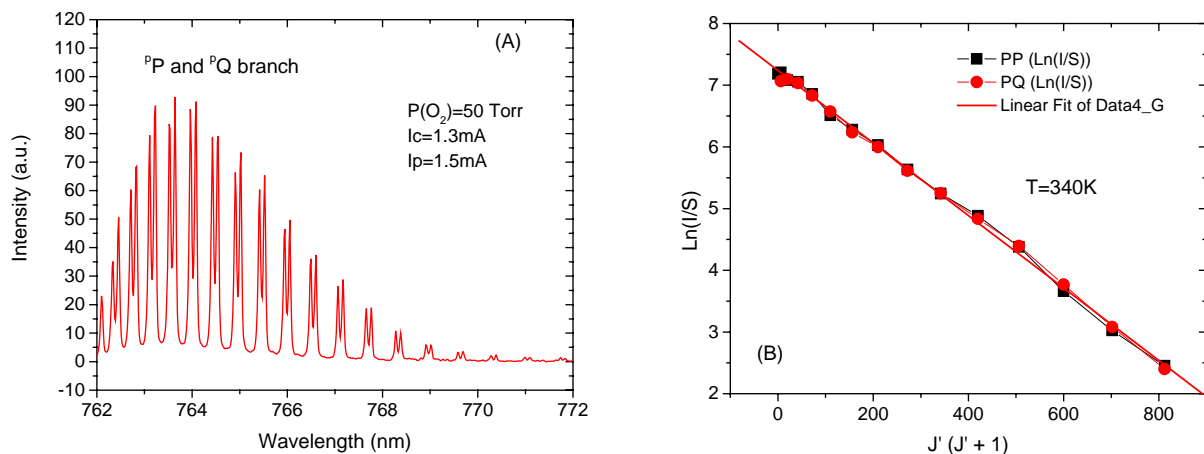
Figure IV-4: High-resolution spectrum of the atmospheric band of oxygen (left) and corresponding Boltzmannn diagram (right).

This high-resolution study confirms our preliminary conclusion based on analysis using the lower resolution system : the plasma in the MCSD is cold. Figure IV-5 shows the measured gas temperature in the MCSD with 50 torr oxygen as a function of current through the MCSD. The gas temperature increases with current but barely exceeds 400 K even for currents up to about 2 mA.   Further, within error bars, there is no variation of the temperature with position in the in the MCSD (the measurements begin at 0.5 mm from the exit of the MHCD).
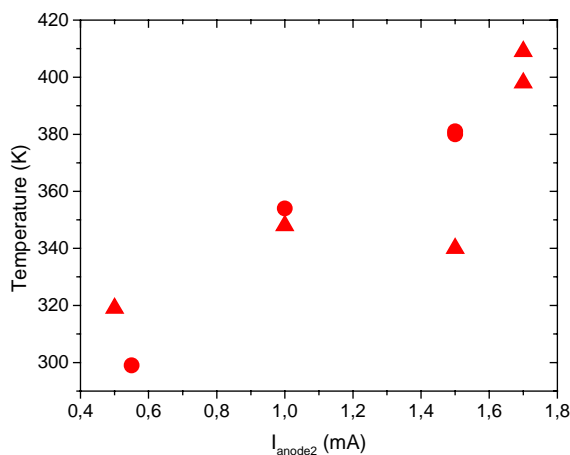
Figure IV-5: Gas temperature in the MCSD as a function of current in 50 torr pure oxygen.

As mentioned above, it is not possible to use this technique to measure gas temperature in the MHCD itself because emission from the atmospheric band is too weak to be seen. In order to get an estimate of the gas temperature in the MHCD, we added a trace of nitrogen to the gas mixture and compared simulated spectra (with gas temperature as a parameter) with measured spectra second positive system at 337.1 nm. Such a comparison is shown in fig. IV-6.
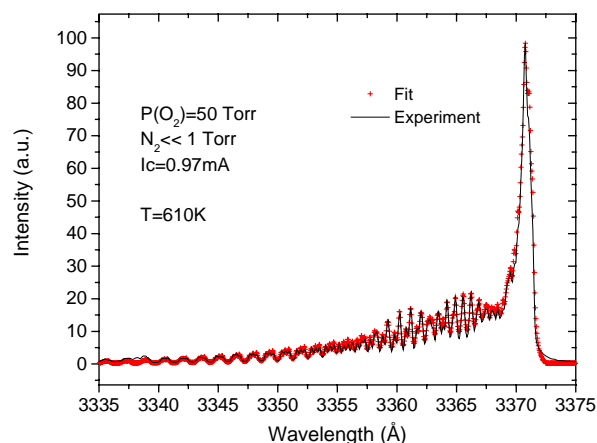
Fig. IV-6. Comparison of measured (black) spectra for the second positive band in nitrogen with a simulated spectrum using a gas temperature of 610 K.

Figure IV-7 shows the gas temperature in the hole of the MHCD deduced from the second positive system of nitrogen. This temperature is higher than those measured in the MCSD, but it is not excessive – it reaches about 620 K for currents on the order of 1 mA.
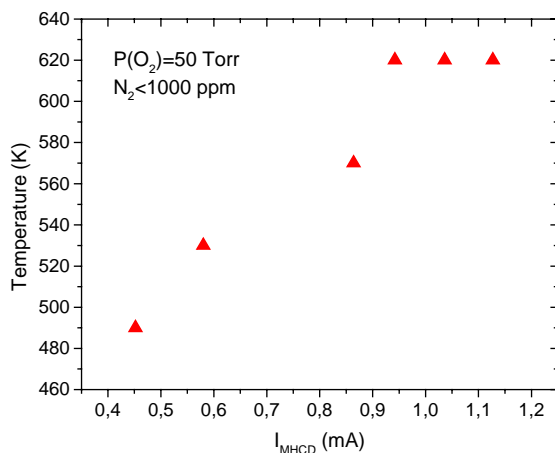
Figure IV-7: Gas temperature in the MHCD vs current

Measurements of gas temperatures in MHCDs have been reported by Miclea et al[6] in argon and helium over a pressure range from 100 to 1000 mbar for MHCDs with a cathode hole diameter ranging from 100 to 300 μm. Our results are consistent with those of Miclea et al - in argon they find a gas temperature in the MHCD of 500 K at 100 mbar, and temperatures increase with gas pressure. The only measurements of the gas temperature in the MCSD that we know of are those of Liepold et al[7], and their operating conditions are sufficiently different from ours that it is hard to make comparisons. In air at atmospheric pressure and for a discharge current of 10 mA, they measure a gas temperature of 2000 K at the mid-plane. The presence of ozone in the MCSD our system (see below) is proof that the upper limit for our gas temperature is at the very most 700 K, at which temperature the ozone would be largely dissociated[8].

Conclusions from spectroscopic study of the 750-780 nm radiation

1/ The atomic line at 777 nm originating from the O*(5p) level is mainly produced in the MHCD. This is clear evidence that the reduced electric field E/N is much lower in the MCSD than in the MHCD. The increase in intensity observed near A2 is consistent with the model and other experimental observations which say that E/N increases in front of A2. In our experimental conditions, the O*(5p) state is mainly produced by electron impact dissociative excitation

$$e + O_2 => O*(5p) + O + e$$
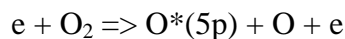
which has a threshold of 15 eV, rather than by electron impact excitation of atoms. The intensity of this line is thus high in regions of high electric field, and it does not give any information about the degree of dissociation.

2/ The atmospheric band with a threshold at 1.8 eV is produced mainly in the MCSD. The emission intensity peaks at about 1.5 mm from the MHCD along the axis of the MCSD and it decreases by a factor of 2 at 2 mm and a factor of 10 in the vicinity of A2.

3/ The absence of signal from the atmospheric band outside the volume of the MCSD indicates that the gas temperatures measured using this emission reflect a local gas temperature in the discharge rather than an average over the reactor volume.

4/ An analysis of the rotational structure of the atmospheric band show that the MCSD is cold : 300 K for currents less than 0.5 mA and about 400 K for currents up to 2 mA. The gas temperature in the hole of the MHCD can reach 600 K, as determined using the 337.1 nm second positive band of nitrogen introduced as a tracer,.

5/ We do not yet have measurements of gas temperature in rare gas/oxygen mixtures, but there are reasons to suppose that the temperatures will be even lower than those measured in pure oxygen. In pure rare gases, the only gas heating mechanism is electron-neutral collisions, which is not very efficient, whereas V-T (vibrational-translational) energy transfer and dissociation cause additional heating in molecular gases. Therefore, diluting oxygen with rare gas will most likely reduce the gas temperature in the MCSD even though the thermal conductivity in argon is lower than in oxygen.

V- Absolute ozone number densities

Ozone is formed in 3-body collisions involving atomic oxygen atoms produced by dissociation of O_2. Since ozone is one of the persistent species produced in discharges containing oxygen, we originally expected to need measurements of its concentration to subtract its contribution to the calorimeter measurements. In addition, ozone and in particular atomic oxygen contribute to the collisional quenching of $O_2(a^1\Delta)$ and $O_2(b^1\Sigma)$, and a measure of the ozone density will be useful in an eventual optimization phase of this project. The ozone density is also a useful quantify for comparison with the model of the MCSD in oxygen and in oxygen containing mixtures.

Ozone absorbs strongly in the UV and its absorption cross section for 253 nm radiation is 1.15×10^{-17} cm^2 (ref. 9). This wavelength conveniently corresponds to a strong line in mercury lamps. By measuring the absorption of the Hg line along a given path length, L, we can directly determine the ozone density through the Beer-Lambert relation:

$$\ln\left(\frac{I}{I_0}\right) = - [O_3].\sigma.L$$

where I_0 is the intensity of the reference source traversing the path length in the absence of a discharge, I is the intensity of the ray with the discharge on, and $[O_3]$ is the ozone number density which we supposed here to be constant along the absorption path length L.

In this way, we have measured the ozone concentration in the reactor and in the measurement cell shown in fig. I-1. The measurement cell is 82 mm long and it is positioned 35 cm downstream from the reactor. The spatial distribution of the ozone in the reactor volume is not known a priori, but we can suppose that it is uniform in the afterglow in the measurement cell. Shown in fig. I-1 is the mercury lamp in the position used for the measurements in the measurement cell. Light emitted from the mercury lamp and passing through the reference cell is collected by a fiber optic placed behind the diaphragm and sent to a spectrometer. Fig. V-1 shows the measured signals in the region of 253 nm when the discharge is on (red curve) or off (blue curve).
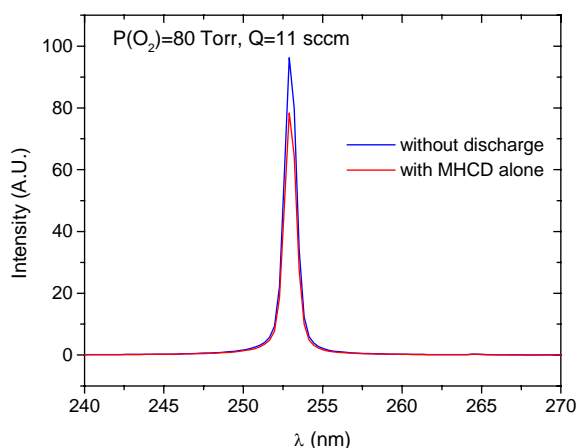
Figure V-1: Radiation from the mercury lamp after passage through the measurement cell with the discharge off (blue reference signal) or on (red).

A series of measurements was performed for discharge currents $I_C = I_{A2} = 1$ mA, in pure oxygen (flow rates from 5 to 40 sccm, pressures between 40 and 120 torr) and in Ar/O_2 mixtures at a total pressure of 50 torr with oxygen partial pressures of 5, 10 and 17 torr. The measurements in the reactor itself were made with a spatial resolution on the order of a mm, and results are reported from the measurement cell along its axis (we suppose that the ozone spatial distribution is homogeneous at this point).

Figures V-2 (pure oxygen) and V-3 (Ar/O_2 mixtures) show the results of these measurements for the conditions as indicated in the figure captions.
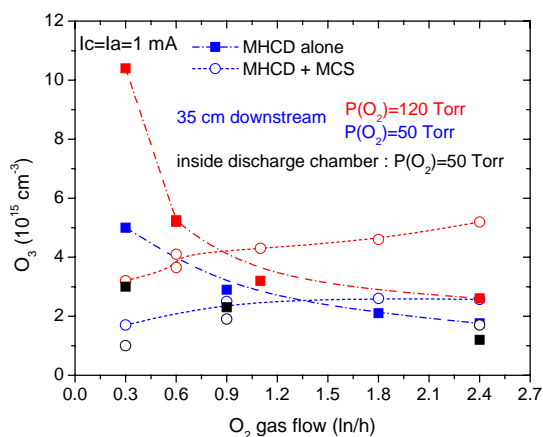
Figure V-2: [O_3] vs gas flow in pure oxygen discharges. Black symbols: measurements inside the discharge chamber, p=50 torr. Blue symbols (50 torr) and red symbols (120 torr) are results in the measurement cell 35 cm downstream. Open symbols : both MHCD and MCSD on; closed symbols – MHCD only.
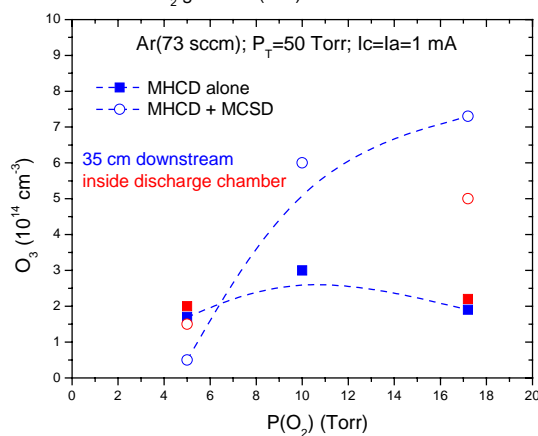
Figure V-3: [O_3] vs partial pressure of O_2 in an Ar/O_2 at 50 torr for $I_C = I_{A2} = 1$ mA. Closed symbols: MHCD only. Open symbols: both MHCD and MCSD on. Red symbols: measurements in the reactor; blue symbols : results in the measurement cell 35 cm downstream.

In pure oxygen and for flow rates less than 25 sccm, (1.5 ln/hr), we find that ozone is uniformly distributed in the reactor volume. We find that the measured concentrations are the same along the discharge axis and 10 mm above (gas inlet) or 10 mm below (gas exit). For higher flow rates, the concentration upstream and on axis are identical whereas the density drops by about 20% at 10 mm off-axis downstream. The gas flow is complicated in the reactor geometry and we cannot suppose it to be the same at each point. In any case, it is clear that the time needed for diffusion is less than the residence time of the gas in the cell for these conditions.

An interesting phenomenon appears at low gas flow rate in pure oxygen: the concentration of ozone measured in both the reactor and in the measurement cell decreases when the MCSD is on. One possible explanation is that ozone is destroyed in quenching collisions with the $O_2(^1\Delta)$ and $O_2(^1\Sigma)$ which are present in the MCSD volume but not in the MHCD. It will be important to understand this point in an optimization phase of this project. A suggestion of

the same phenomenon is seen in the mixture in fig. V-3, although the precision of the measurement for 5 torr oxygen is limited.

VI. Absolute atomic oxygen number densities

The results presented in this section were obtained using the Laser Induced Fluorescence (LIF) system of Lionel Magne at Orsay.

The principle of the method for making absolute measurements of [O] using 2-photon LIF has been described by Döbele et al[10]. Briefly, the method is based on the calibration of the LIF signal in oxygen with that obtained in xenon, which is introduced with a known density in the reactor. The near coincidence in energy of the upper level of xenon (excitation by 2 photons at 224.31 nm) and of atomic oxygen (excitation by 2 photons at 225.65 nm) and the similar wavelengths of the fluorescence signals detected (844.87 nm for oxygen and 834.91 nm for xenon) allow calibration of the pumping laser and detection system.   The calibration is valid over a range of laser power levels but only in pure oxygen.

The LIF system in Orsay consists of a Datachrom 5000 Quantel pulsed Nd :YAG laser, a tunable dye laser, and a UV generation stage. The Nd :YAG radiation at 1064 nm frequency doubled to obtain radiation at 532 nm. This radiation pumps the dye laser tuned to produce 572 nm radiation. The 572 nm radiation is then frequency doubled and mixed with IR at 1064 nm from the Nd :YAG laser to produce a 7 ns laser pulse at 225 nm with a frequency of 10 Hz. The available laser energy at 225 nm is about 2 mJ per pulse. This energy is attenuated for the measurements to insure that loss of the upper level due to photoionization is negligible. Typically, we use 40 to 60 µJ per pulse for the measurements in oxygen and 10 µJ or less per pulse for the calibration in xenon.   We have confirmed that there is no saturation for these laser pulse energies.

Figure VI-1 shows a schematic of the geometry of the laser beam and the detection arrangement. The fluorescence signal is collected by a lens of BK7 with a 75 mm focus perpendicular to the laser beam. To select the fluorescence signal of interest, an interference filter centered at 850 nm with 25 nm band pass is placed in front of a photomultiplier.

The fluorescence signal is integrated in time by a boxcar synchronized with the laser beam. The measurements presented here were all made in oxygen at 50 torr.

Figure VI-1 : Schematic of the LIF system. The anode A2 is the upper black plane and the MHCD is the lower plane.
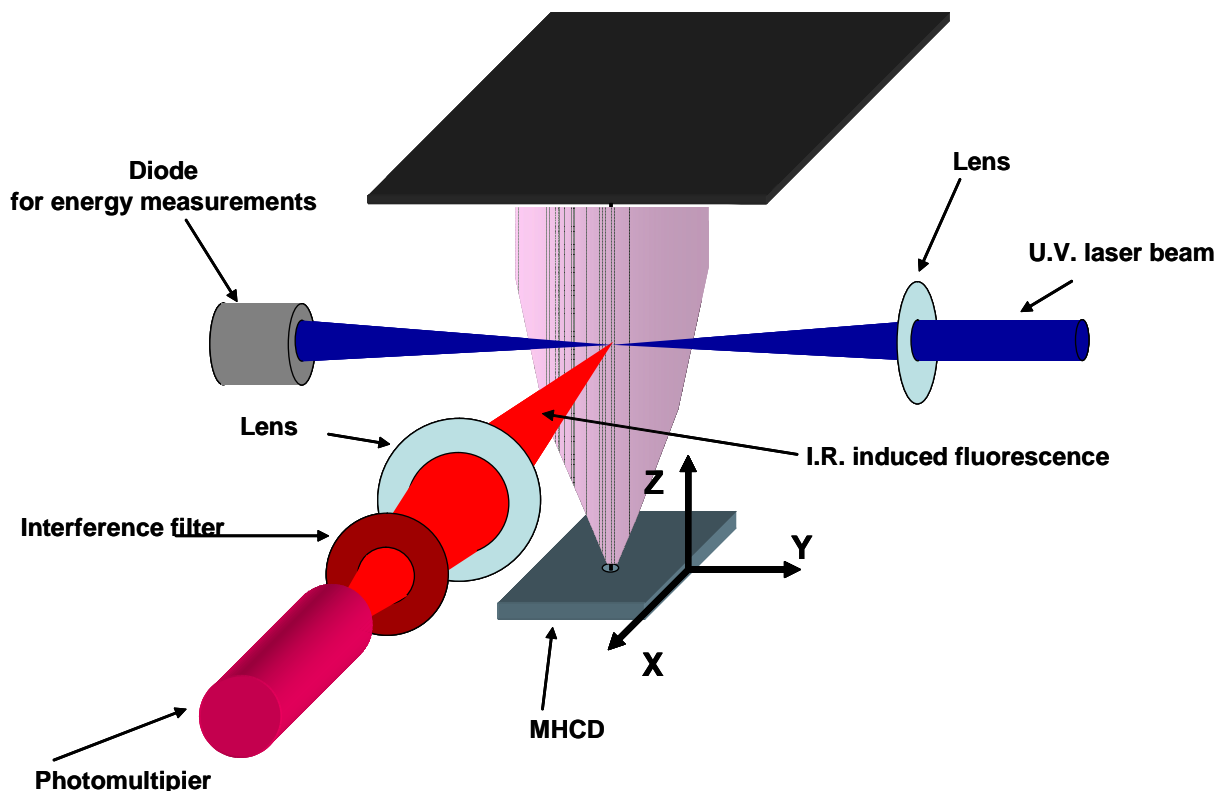
The reactor was mounted on a system to allow translations in both axial (Z) and radial (X, in the figure) directions with respect to the laser beam which is fixed. The spatial resolution, estimated to be about 50 µm is given by the beam waist at the focal point of the lens.

Figure VI-2 : Axial profile of [O] with and without MCDS discharge on.
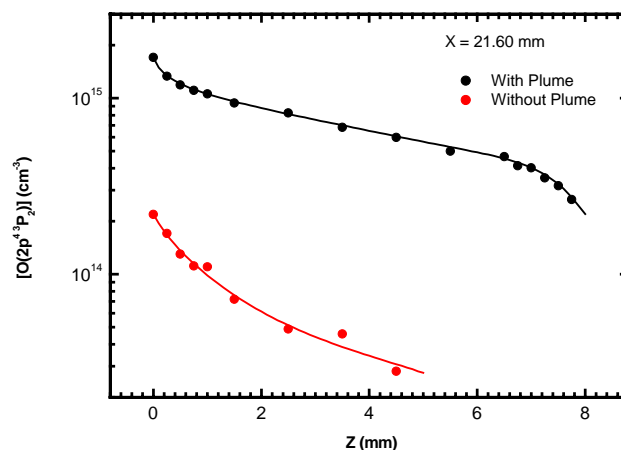
Figure VI-2 shows profiles of ground state oxygen atom number density along the axis of the MCSD in absolute units for a discharge in pure oxygen at 50 torr and for a flow rate of

0.1/minute (150 sccm). The current in the MCSD was 1 mA and the plasma in the MCSD region was perfectly stable. The laser energy for these measurements was 60 µJ per pulse.

The atomic oxygen number density decreases slowly with axial position and then more rapidly in front of anode A2. We turned off the MCSD, keeping the MHCD on, and repeated the measurements with the result shown in the lower curve in fig. VI-2.   The [O] produced in the MHCD and diffusing into the MCSD volume (discharge off) are a factor of 10 or so less than with the MCSD also powered. Thus the measurements reported are indeed due to [O] production in the MCSD.
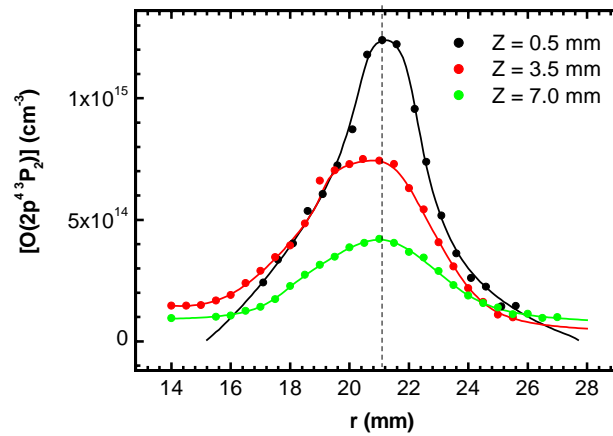
Figure VI-3 : Radial profiles of [O].

Radial profiles of [O] are shown in fig.VI-3 for three different axial positions ; close to the MHCD, at the mid-plane of the MCSD, and very near the electrode A2. The width of the profiles increases slightly with axial position, and there is a suggestion of a shift of the mid-plane profile towards the direction of the gas flow at the middle position.
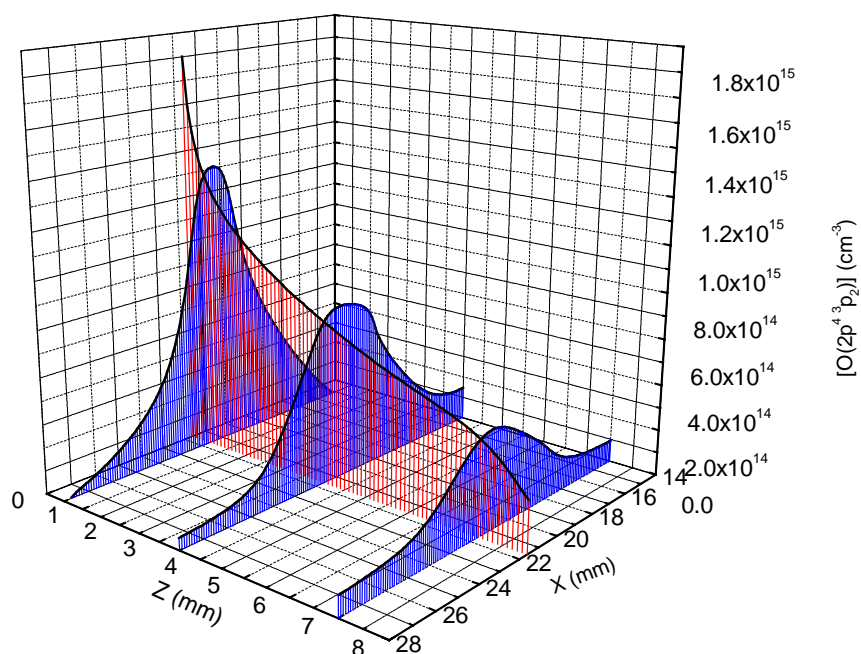
Figure VI-4 : Summary of [O] measurements. Z=0 is the exit plane of the MHCD.

VII. Detection of O$_2$(a$^1\Delta$) using fluorescence at 1.27 μm

The fluorescence at 1.27 µm resulting from the radiative deexcitation of the O$_2$(a$^1\Delta$) is the only diagnostic we have at this point to demonstrate that microdischarges can indeed be used to generate high yields of O$_2$(a$^1\Delta$). We had originally intended to use this simply as a check of the calorimeter system, and so the system was available when we realized that the calorimeter measurement was not functioning as expected.   The extraction of the weak signal at 1.27 µm proved challenging and required considerable effort to measure and calibrate. The yields inferred from the fluorescent signals are impressively high, especially since no effort has yet been made to optimize the discharge for this purpose.   *While these results are very promising, it is important to emphasize they need to be validated by comparison with other diagnostic techniques.*

Another point to emphasize is that we do not yet understand all the results obtained. A better understanding will require more time and further experiments and modeling. Our purpose has been to demonstrate production of O$_2$(a$^1\Delta$) in microdischarges, and we have been successful in this, but there is much more to be done to fully understand our results.

Experimental set-up

A liquid nitrogen cooled, InGaAs detector was positioned at one of two points : either at the side window of the reactor as shown in fig. I-1 or in place of the mercury lamp shown in fig. I-1, at a position 2.5 cm from the flat face of the measurement cell. Recall that the measurement cell was positioned 35cm downstream from the reactor and after the calorimeter for most of these measurements. A few results were obtained with the measurement cell located at 23 and at 48 cm downstream.

A narrow-bank interference filter (Andover 200FC39-25/1270) with 19 nm band pass selected the emission centered on 1.27 µm. We confirmed that the emission signal was completely eliminated when we replaced the filter centered at 1.27 µm with another (Andover 120FS10-25) centered 1.20 µm with 11.6 nm band pass. Thus, the signal seen by the InGaAs detector corresponds to either an atomic line or a molecular band and not to a background continuum. The detector signal is amplified by an op-amp with a gain of 10^7 before arriving at the oscilloscope. Because of the very long radiative lifetime of 4424 s of the O$_2$(a$^1\Delta$) state[11], the extraction of the 1.27 µm signal from the background noise is difficult. This difficulty is evident in fig. VII-1, which shows the raw signal detected with the discharge on (blue) and off (black).
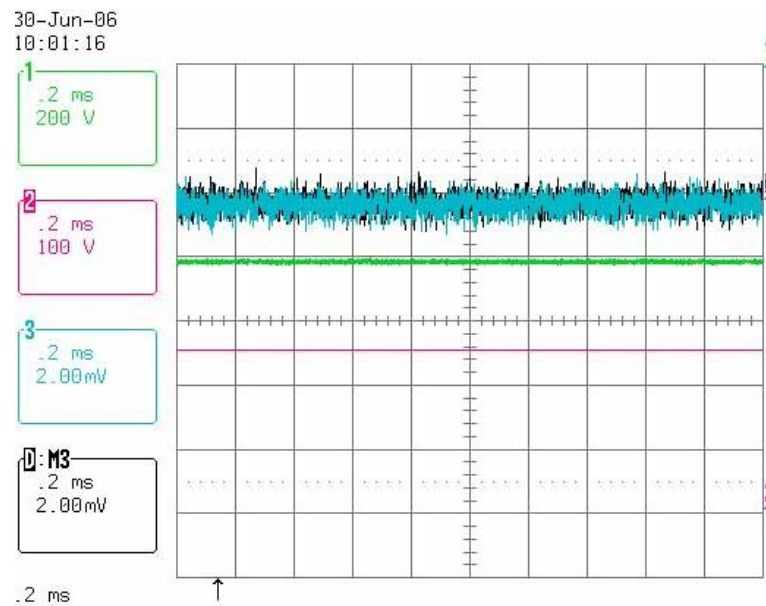
Figure VII-1: Comparison of raw data from the InGaAs detector positioned next to the reactor with the discharge on (blue) or off (black).

In order to extract the signal from the noise, we developed a correlation technique, pulsing the MCSD by applying a square wave voltage and averaging over a large number of cycles. The main discharge - the MHCD - is ON continuously. The square wave voltage ON and OFF periods are separately adjustable over a range of 0.1 ms to 1 s, and the oscilloscope was triggered either by the square wave, or by the rising current or voltage drop in the MCSD. Figure VII-2 shows the results after averaging over 200 discharge ON/OFF periods. Although the raw data signal (blue trace) only hints at a modulation on a 2 mV/division scale, the averaged signal (black trace) from the InGaAs detector is clearly modulated as the MCSD is switched on and off.
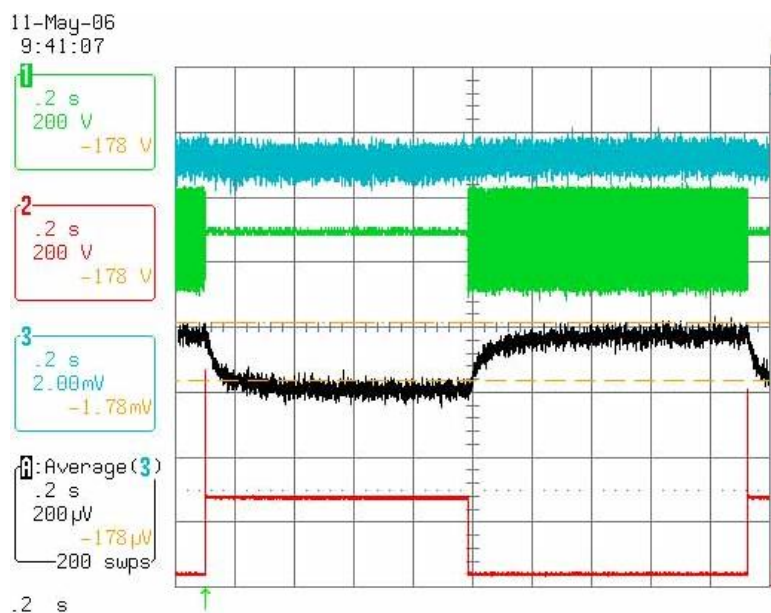
Figure VII-2: Oscilloscope traces corresponding to pulsed MCSD ($T_{ON}=T_{OFF}=0.9s$) in pure oxygen at 75 torr, with the InGaAs detector in position next to the reactor window.
The blue trace on the top is the raw signal from the InGaAs detector on a scale -2 mV/division and the black is the signal averaged over 200 periods on a scale of -200µV/div. The green trace is the MHCD voltage on a scale of 200 V/division, and the red trace is the MCSD square wave voltage also on a scale of 200 V/div.

The voltage needed to initiate the MCS discharge in these conditions is about 700 V. After the MCSD is initiated, the voltage drops quickly to a rather constant value. The InGaAs detector signal is modulated in phase with the square wave voltage, but requires about 0.1 s to arrive its steady-state value after MCSD initiation and somewhat longer to return to its initial value when the MCSD is switched OFF. When the MCSD is initiated, there is an abrupt change in the MHCD discharge which makes a transition from the self-pulsing regime to a constant voltage regime. The thick part of the green trace in the figure VII-2 corresponds to a series of voltage peaks which is the signature of the self-pulsing region of MHCD operation. We have previously observed and studied in some detail a self-pulsing regime. This phenomenon is not described in detail here, but two articles[4] - one published and one submitted for publication – describe in detail the phenomenon of self-pulsing in MHCDs in pure argon. Briefly, the self-pulsing regime is manifested as periodic (10 to 100 kHz) current or voltage pulses associated with expansion and extinction of a plasma on the back face of the cathode. We do not yet understand the reason for the interference between the MCSD and the self-pulsing in the MHCD, preferring to concentrate fully for the moment on the exploitation of the plasma in the MCSD volume for the generation of $O_2(a^1\Delta)$.

A factor complicating the measurement in Ar/O_2 mixtures is interference from the strong atomic argon lines $3s^23p^5(^2P_{1/2})4p$ - $3s^23p^5(^2P_{1/2})3d$ and $3s^23p^5(^2P_{3/2})4p$ -$3s^23p^5(^2P_{3/2})3d$, which radiate in the wavelength interval passed by the filter and hence mask the signal from $O_2(a^1\Delta)$. It is could eventually be possible to distinguish these signals on the basis of their difference time dependencies. Emission from the $O_2(a^1\Delta)$ state responds much more slowly to changing conditions than do the argon lines. This is shown in the green line (upper trace) in fig. VII-3 where the same detection system is used to look at a plasma in pure argon at 75 torr. Looking more closely at the time dependence of this signal, we find that its response time is limited by the response time of the op-amp, 1 ms.

Another difference between the signals in argon and in oxygen is in the degree of modulation with MCSD ON/OFF. In argon, the InGaAs signal is easily distinguished from the background noise, but there is little difference in its amplitude between MCSD ON and OFF. That is, in argon the MHCD itself is a strong source of radiation in the band pass of the filter, whereas essentially no signal is observed from the MHCD alone in oxygen discharges. Thus we conclude that the $O_2(a^1\Delta)$ is produced only in the MCSD.
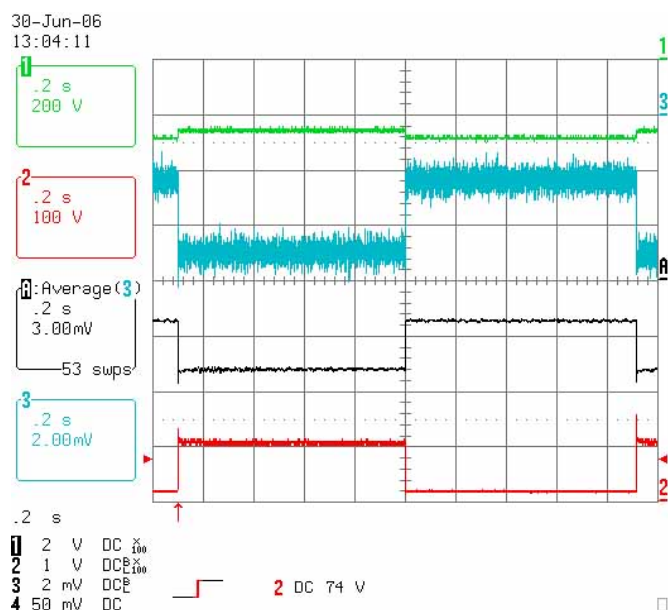
Figure VII-3: Oscilloscope traces showing the InGaAs detector signal from a pulsed MCSD ($T_{ON}=T_{OFF}=0.9s$) in pure Ar (P=75 Torr).
The blue trace is the raw data from the InGaAs detector and the black signal is the signal averaged over 200 cycles. The green and red signals are the voltages to the MHCD and MCSD respectively.
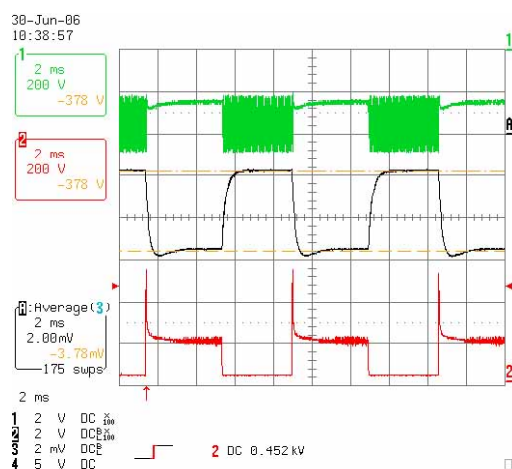
Figure VII-4: Same as fig. VII-3 but for a shorter period ($T_{ON}=T_{OFF}=4$ ms)

In order to quantify the $[O_2(a^1\Delta)]$ using the emission signals in pure O_2 discharges where there is no spectral interference, we need information about the spatial distribution of this

36

species. As discussed in Section IV the radiating species $O_2(b^1\Sigma)$ is fairly well localized along the discharge axis, but the same cannot be assumed for the $O_2(a^1\Delta)$. Nor can we suppose that the $[O_2(a^1\Delta)]$ is uniform throughout the reactor volume. A very rough estimate of the residence time of an O_2 molecule in the plasma region gives the same value as an equally rough estimate of the diffusion time constant (on the order of 1 ms). Both are complicated by the reactor geometry. The complex gas flow and diffusion in our reactor geometry thus prevent our extracting yield information from the emission signals with the detector positioned next to the reactor.

The situation is much simpler if we position the detector at the flat face of the measurement cell shown in fig. I-1. Again, measurement cell is 35 cm downstream from the reactor and the gas flow in this part of the system is expected to be homogeneous, unlike in the reactor itself. If we make the reasonable assumption that the spatial distribution of the $O_2(a^1\Delta)$ in the measurement cell is homogeneous, we can calculate the probability of a photon reaching the detector surface using a Monte Carlo simulation. For our geometry, this figure is $1.9 \ 10^{-4}$. The geometry of the measurement cell is as follows : 14 mm diameter, 82 mm length, effective window diameter 11 mm, and of the detector : 3 mm diameter circular surface and 60° collection angle, with the distance from cell window to the detector : 25 mm. Other figures needed for calibration are the sensibility of the photodetector (0.9 A/W), the gain of the amplifier (10^7), the filter transmission at 1.27 µm (35 %). Taking all these factors into account, 1 µV of signal detected corresponds to a number density of $3.7 \ 10^{12} \ O_2(^1\Delta)/cm^3$ in the measurement cell.

Initial results in pure oxygen were quite disappointing : with the measurement cell positioned behind the calorimeter, we detected no 1.27 µm photons from discharges in pure oxygen. In retrospect, this is not surprising because the lowest pressure that can be used in our reactor is 25 torr and quenching of $O_2(a^1\Delta)$ in collisions with ozone or atomic oxygen (in which case the collisions are 3-body collisions) will destroy all or most of the $O_2(a^1\Delta)$ during the transit from the reactor to the measurement cell. Experiments at lower pressures are not possible in our present system - the lower limit on the pressure is due to the design of the MHCD itself and could be lowered with another design.

The situation is better in mixtures of rare gas and oxygen and it is here that we measure high yields. Before working with Ar/O_2 mixtures, we first verified that there is no detectable signal in the measurement cell from pure argon discharges. The radiative lifetime of the states in the $3s^2 3p^5(^2P_j)3d$ configuration is shorter than the time needed for the gas to flow the 35 cm from the reactor to the measurement cell. This time is about 0.15 seconds for the highest flow rates used in our experiments and considerably longer than the radiative lifetime (< 1 µs) of the states than can emit in the band pass of the 1.27 µm filter. Thus, we are confident that the observed signal from the InGaAs detector is due to emission from the $O_2(a^1\Delta)$ still present downstream from the reactor. The densities we infer at this point underestimate the densities in the reactor itself because of losses along the way.

[$O_2(a^1\Delta)$] downstream in Ar/O_2 and He/O_2 mixtures

Figure VII-5 shows the evolution of the IR signal and the corresponding $O_2(a^1\Delta)$ number density as functions of total gas pressure in an Ar/O_2 mixture with 5.9% oxygen. For these experiments, the currents in the MHCD and in the MCSD were fixed at 0.5 mA. The four curves shown in the figure correspond to four different gas flow rates.
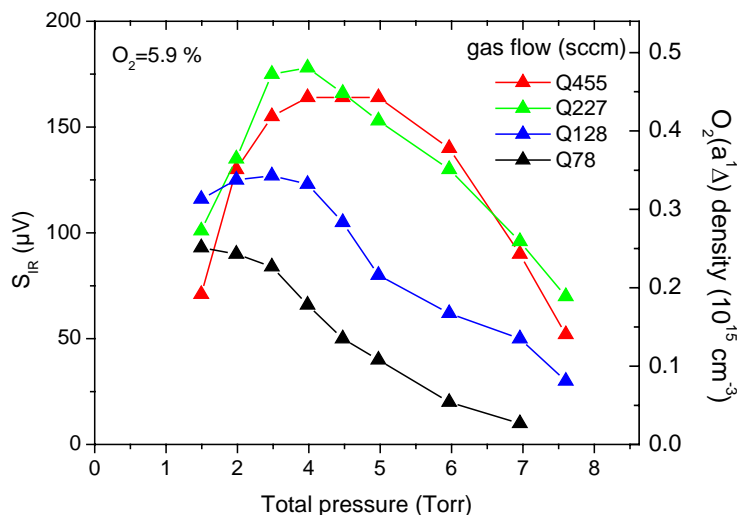
Figure VII-5: IR signal and corresponding $O_2(a^1\Delta)$ density as a function of pressure in Ar/O$_2$ mixtures with 5.9% O$_2$ and for $I_C = I_{A2} = 0.5$ mA.

The four curves correspond to four different gas flow rates.

For the lowest gas flow rate, 78 sccm, $[O_2(a^1\Delta)]$ reaches a maximum at about 0.3 10^{15} cm^{-3} for the lowest total gas pressure and it decreases rapidly with increasing pressure. Higher values for $[O_2(a^1\Delta)]$ are obtained with higher flow rates and reach almost 0.5 10^{15} cm^{-3} for 227 sccm. For these conditions, we see a shift of the peak in $[O_2(a^1\Delta)]$ towards higher total gas pressures. The densities are independent of gas flow for flow rates greater than about 200 sccm - the results obtained for 227 and 455 sccm are equal within estimated error. The reproducibility of these results is estimated to be about 25% and is due mainly to a limited control on the gas flow. This precision could be considerably improved by replacing our manually operated valves and flow meters with electronic controllers. For flow rates greater than 200 sccm, the maximum value of $[O_2(a^1\Delta)]$ is obtained for a total gas pressure of 60 torr, corresponding to a partial pressure of O$_2$ of 4 torr. For higher pressures, the density decreases independent of the flow rate. The observed dependence on both gas flow and total pressure are consistent with collisional quenching during the transport to the measurement cell.

Further work is clearly needed to establish exact quenching processes. In a first attempt towards this end, we have tried to separate the relative effects of oxygen and of argon by fixing the partial pressure of oxygen at 5 torr and varying the argon pressure and gas flow rate. Figure VII-6 shows that for gas flows greater than 200 sccm, the argon partial pressure has only a weak influence on $[O_2(a^1\Delta)]$. A slight maximum appears at about 70 torr argon as the argon pressure increases from 20 to 70 torr. On the other hand, the argon partial pressure has a significant effect on the IR signal for low gas flow rates - at 73 sccm an increase in the argon pressure from 20 to 128 torr leads to a drop of an order of magnitude in $[O_2(a^1\Delta)]$. Clearly, quenching of $O_2(a^1\Delta)$ in processes involving argon (in particular, $O_2(a^1\Delta)+O+Ar$) is playing a role during the transport from the MCSD to the measurement cell. More work is needed to understand these results.
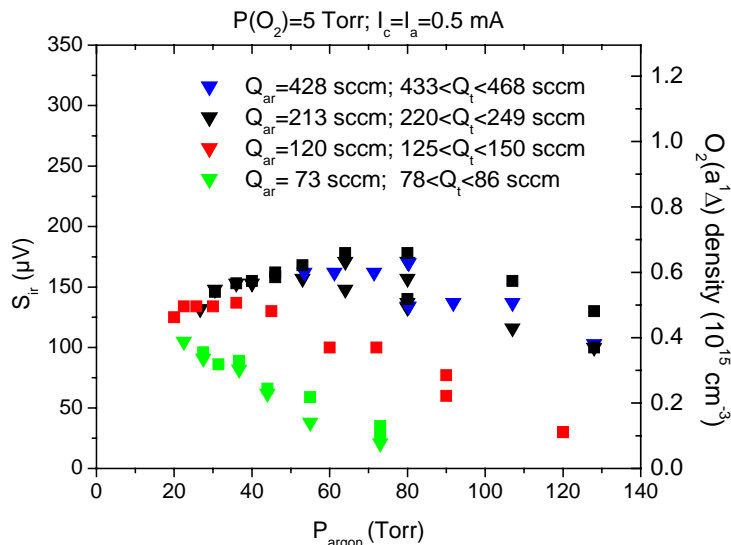
Figure VII-6: IR emission signal and corresponding [$O_2(a^1\Delta)$] vs argon pressure for 4 different gas flow rates with 5 torr oxygen partial pressure $I_C = I_{A2} = 0.5$ mA. Different symbols in the same color are used to indicate measurements on different days and to show the reproducibility.

Shown in fig. VII-7 are measured IR signals as a function of oxygen partial pressure for three different values of the argon partial pressure, 50, 75 and 112 Torr. These measurements were made for a gas flow rate of 429 sccm, a flow rate fast enough to compensate the effect of quenching by argon as seen above.
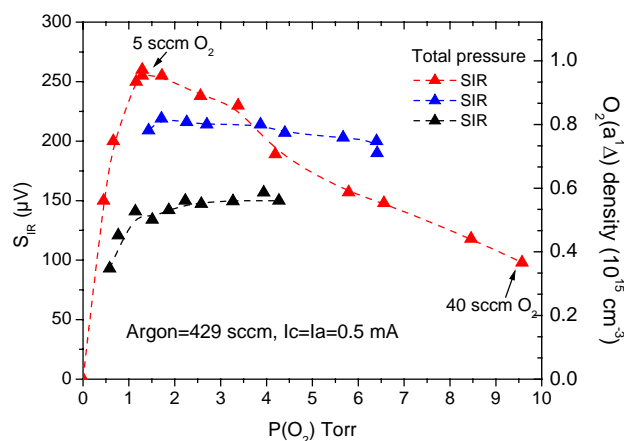
Figure VII-7: IR signal and corresponding $O_2(a^1\Delta)$ density as a function of oxygen partial pressure for 3 different pressures of argon. $I_C=I_{A2}=0.5$ mA

For these conditions, [$O_2(a^1\Delta)$] increases with oxygen partial pressure up to about 1.5 torr. For 50 and 75 torr argon, [$O_2(a^1\Delta)$] is approximately constant between 1.5 and at least 6 torr O2. However, for 112 torr argon, an increase in the oxygen partial pressure past 1.5 torr leads to a drop in [$O_2(a^1\Delta)$].

Another point that we checked in one set of experiments is the influence of the reactor cell geometry. The windows allowing optical access to the MHCD and MCSD regions require a cell volume considerably larger than the discharge volume itself. For comparison, the volume of the MCSD is about 0.2 cm^3, much smaller than the volume occupied by gas in the reactor,

39

21 cm^3. In our reactor geometry, we do not expect the gas flow to be homogeneous, and thus it is difficult to estimate what fraction of the input gas actually passes through the discharge zone. Any gas not passing though the discharge region will only dilute the yield of $O_2(a^1\Delta)$. To check the possible importance of this effect, we reduced the reactor volume to 2.5 cm^3 by blocking the optical access. Reducing the reactor volume by a factor of 8.4 did not influence the IR signal observed in the measurement cell, as we show in fig. VII-8. Neither did this modification in the reactor volume influence the electrical properties of the discharge.
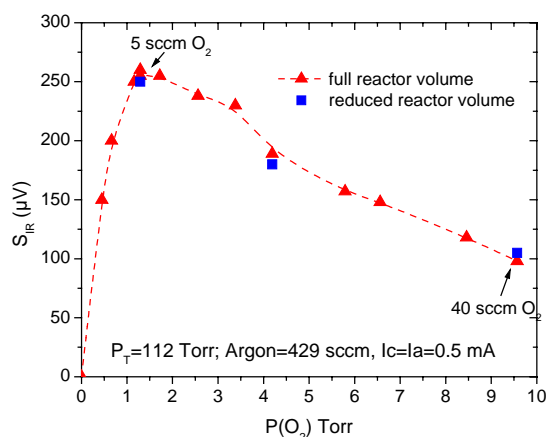
Figure VII-8: Comparison of the IR signal measured in the large volume (red triangles) and small volume (blue square) reactor configurations.

A few experiments were done to determine $[O_2(a^1\Delta)]$ in mixtures of helium and oxygen; this gas mixture has been used in previous work. Figure VII-9 shows a comparisons of $[O_2(a^1\Delta)]$ generated in argon/oxygen and in helium/oxygen mixtures. For a total gas pressure of 112 torr and similar gas flow rates in the two mixtures - 433 sccm with helium and 429 sccm with argon - the nature of the rare gas in the mixture has a large influence on the dependence of the $[O_2(a^1\Delta)]$ with oxygen partial pressure. In He/O_2, $[O_2(a^1\Delta)]$ increases with O_2 concentration over the entire range investigated, with a suggestion of a saturation effect above about 6 torr, whereas in Ar/O_2 there is a clear maximum at about 1.5 torr. Of course the electrical characteristics of the discharge also depend strongly on the nature of the rare gas, as was shown about in Section II.
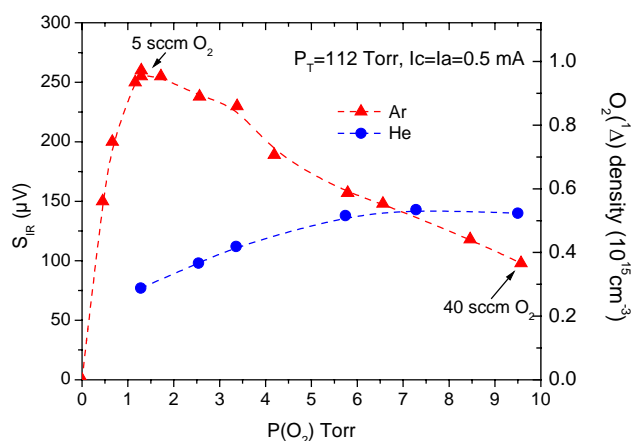
Figure VII-9: IR signal and [O$_2$(a$^1\Delta$)] vs oxygen partial pressure from He/O$_2$ and in Ar/O$_2$ discharges.

For the conditions studied so far, the maximum O$_2$(a$^1\Delta$) yield is greater in Ar/O$_2$ mixtures than in the He/O$_2$ mixtures except for high partial pressure of O$_2$. For the conditions of fig. VII-9, in the He/O$_2$ mixture, the maximum [O$_2$(a$^1\Delta$)] we have measured is about 0.5 10^{15} cm^{-3} whereas a maximum density in the Ar/O$_2$ mixture is twice that.

Considerable optimization is possible. For example, measurements as a function of discharge current are shown in fig. VII-10 in Ar/O$_2$ at 112 with 1.3 torr of O$_2$. The [O$_2$(a$^1\Delta$)] density increases with current and reaches 3 10^{15} cm^{-3} for a discharge current of 4 mA, as measured at a point 23 cm downstream from the reactor. This [O$_2$(a$^1\Delta$)] density corresponds to a fractional concentration of 7.6% in the measurement cell if we suppose a gas temperature of 300K. This clearly represents a lower limit to the [O$_2$(a$^1\Delta$)] yield in the reactor itself for these conditions. We have not yet explored a wide enough range of conditions to establish an upper limit to the yield possible in these microdischarge configurations.
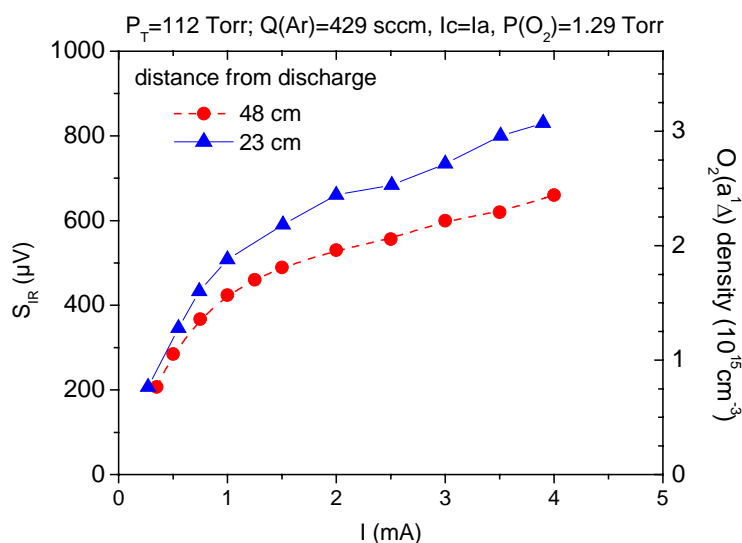
Figure VII-10: IR signal and inferred [O$_2$(a$^1\Delta$)] as a function of discharge current for a gas mixture Ar/O$_2$ with 1.29 torr O$_2$ and a total gas flow rate of 429 sccm.

41

Conclusion : The $[O_2(a^1\Delta)]$ measured in the measurement cell 23cm downstream from the reactor correspond to yields of up to 7.6 %. This figure represents a lower limit for the yield in the reactor itself because of losses during transport. While these measurements have been made with considerable care and attention to detail, it is important to emphasize again the need for experimental confirmation via other diagnostic techniques. In any case, microdischarge configurations are promising sources for high yields of $[O_2(a^1\Delta)]$.

VIII- Parallel operation of four microdischarges

In this section we will present some first results to show the possibility of scaling up to larger volumes by operating several MCSDs in parallel. The group of Schoenbach[12] succeeded in operating two parallel MCSDs in air at atmospheric pressure, but they do not appear to have developed this concept in much detail. In addition to scaling up in volume, parallel operation may offer the possibility of increasing the yield of $O_2(a^1\Delta)$; the saturation observed in fig. VII-11 with increasing current suggests that the increasing yield cannot be achieved by increasing the discharge current. To test this concept, we designed and build a new discharge in which 4 MCSDs, each with its own MHCD, can be operated in parallel. Given the time constraints imposed by this contract, we have simply shown that parallel operation is possible. This first prototype is sufficient to visualize the discharges, but no additional diagnostics have yet been made. This prototype was designed so that the measurement cell and the infrared detector can be positioned at the gas exit, but this has not yet been tested.

Figure VIII-1 shows a schematic of the discharge cell with the four MHCD sandwiches and four separate anodes A2 for the MCS discharge. As for the reactor described in the previous section, the distance between the MHCDs and the anodes A2 is 8 mm and the distance between each MHCD is about 6 mm
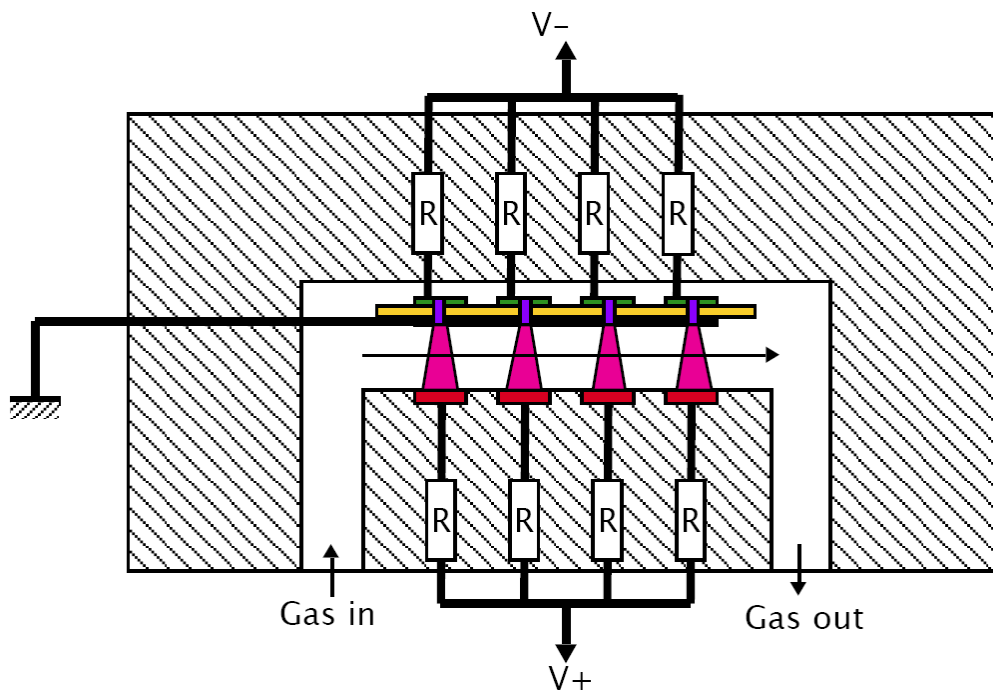
Figure VIII-1: Schematic of the prototype reactor with 4 MCSDs, each controlled by a separate MHCD.

Photographs of the four discharges in mixtures of Ar/O_2 with 5% O_2 at a total pressure of 75 torr are shown in figs. VIII-2 to VIII-5. These figures show the visual appearance of the discharge for the following test cases : (fig. VIII-2) we first demonstrated that it is possible to operate the 4 MHCDs in parallel without initiating the MCSDs. (fig. VIII-3) :With all 4 MHCDs on, it is possible to select and turn on only one MCSD. (figs. VIII-4 and VIII-5) : All four MCSDs are functioning in parallel. In all cases, the MCSDs were completely controlled by the MHCD - that is, when the MHCDs are extinguished, so too are the MCSDs.
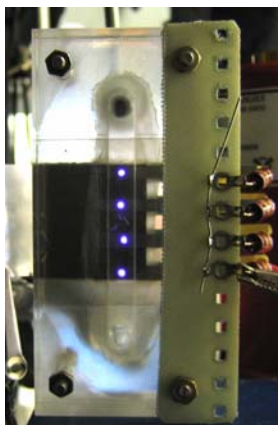
Figure VIII-2 : Parallel operation of four MHCDs with hole diameter 200 µm and dielectric thickness 150 µm. The distance between the MHCDs is 6 mm. Discharge in Ar/O_2 with 5% O_2 at a total pressure of 75 torr. The current through each MHCD is 1 mA, for a total current of 4 mA.
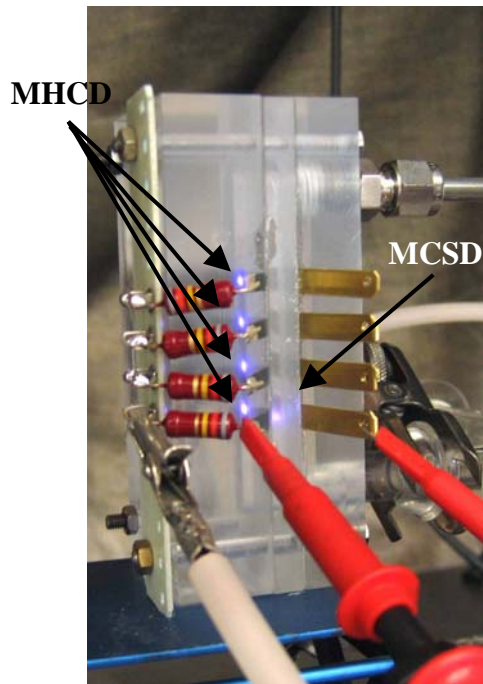
Figure VIII-3: Parallel operation of four MHCDs with one single MCSD in operation. Same conditions as in fig VIII-2.

Figure VIII-4: Parallel operation of 4 MHCDs with all 4 MCSD operating. Same conditions as in fig VIII-2.
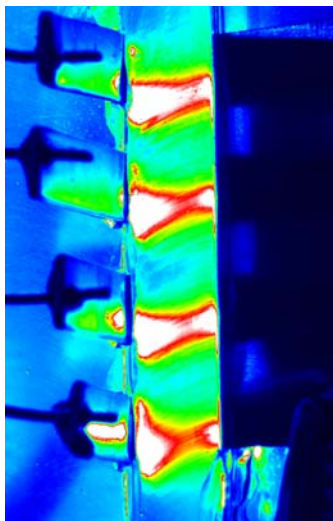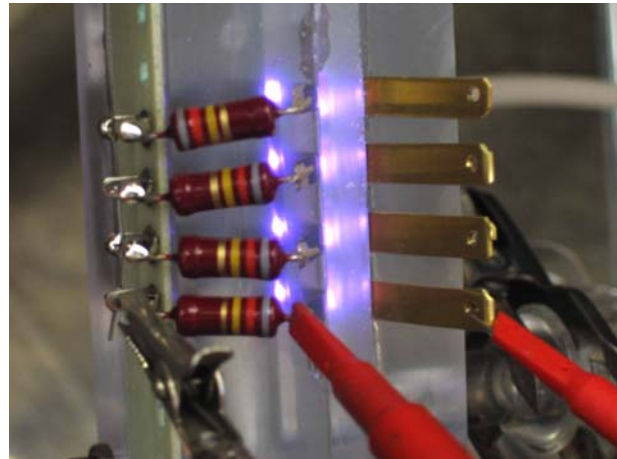
Figure VIII-5: A false color image taken with a CCD camera to show the 4 MCSDs operating in parallel. Same conditions as fig. VIII-4.

IX. Numerical Model

Description of the model

We have developed a 2D model (cylindrical symmetry is assumed) to study the properties of the plasma in the MCS region. The objective of our modeling work is to provide a framework for understanding the physics of the MCSD and to provide a tool to help guide the experimental optimization of the discharge conditions.

As discussed above, we concluded in our report of December 2005 that the plasma in the MCS region is essentially a radially expanding positive column. So, the situation we aim to model is the radial expansion of the current conducting channel from the exit plane of the MHCD to the anode A2. Quasi-neutrality is imposed and the two-dimensional, self-consistent electric field distribution is determined such as to insure current continuity. The complicating factor is that the details of the plasma chemistry in oxygen mixtures must be taken into account to predict correctly the plasma conductivity. This must be done self-consistently because rates for processes involving the electrons depend on the local E/N.

The model is based on the solution of continuity equations for the charged particles coupled to the current conservation equation for the determination of the electric field. Neutral species are also described by their continuity equations. The variables are thus the electric field and the species number densities, and these are functions of time and of axial and radial spatial coordinates. It is the steady-state solution that is of interest for the moment. The computational volume includes the entire MCS space and the boundary conditions are as follows : a fixed current crossing the part of the boundary corresponding to the exit of the MHCD, zero gradients at the radial boundaries, fixed potential on the third electrode A2, and neutral and charged particle densities at the third electrode depending on the assumed reflection coefficients. Gas heating due to the electron current has been included and shown to be negligible in argon, but gas heating in molecular gases can result from excitation or dissociation and thus we expect a slightly higher temperature in the oxygen containing mixtures. However, for the moment this is neglected in our models. The justification for neglecting gas heating is that the measurements of the gas temperature in pure oxygen discharges in MCS region reported above show that the increase in gas temperature is limited, with a peak temperature at less than 400 K for currents less than 2 mA.

The computational volume is shown in fig. IX-1.
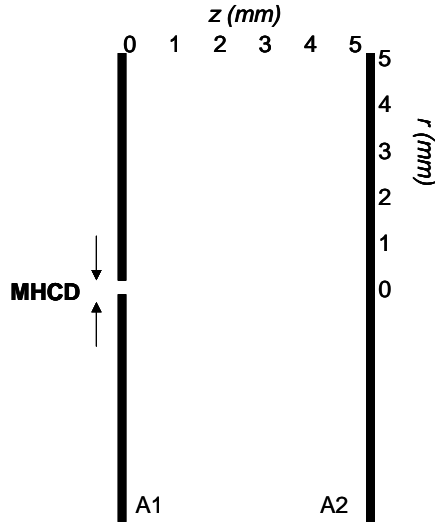
z (mm)

0　1　2　3　4　5

r (mm)

MHCD

A1　　　　A2

Fig. IX-1. Computational volume used in the model. The anodes A1 and A2 are shown, and a current source is imposed at radial positions corresponding to the MHCD in the plane of A1. Actually, only half of this volume is included in the model, cylindrical symmetry being assumed.

First results

<u>Pure argon :</u> The model has been used to obtain results in argon discharges for direct comparisons with the experiments of our partner Antoine Rousseau. Since these comparisons serve mainly to validate the model and are not directly related to the $O_2(^1\Delta)$ application, we will not detail the argon results here. Suffice it to say that detailed comparisons with experiments are underway and agreement is so far quite reasonable.

<u>Ar/O_2 mixtures</u> : We have concentrated our modeling effort on mixtures of Ar and O_2 and first results are now available for direct comparison with experiments. The species included explicitly in our calculations in this mixture are :

8 Charged particle species : e^-, O_2^+, O_4^+, O^-, O_2^-, O_3^-, Ar^+ and Ar_2^+

8 Neutral particle species : O_2, $O_2 (^1\Delta)$, $O_2 (^1\Sigma)$, O_3 , O , $O(^1D)$, Ar, and Ar^*

The kinetic scheme used for our calculations is based mainly on previous results from Stafford and Kushner[12]. About 100 reactions are considered, and the main difference between our kinetic scheme and that of ref. 12 is the inclusion of 3-body quenching collisions for the $O_2(^1\Delta)$, and in particular the following reactions;

$$O_2(^1\Delta) + O + Ar => O_2 + O + Ar \qquad\qquad k = 6.3 \ 10^{-39} \ cm^{-3}$$

$$O_2(^1\Delta) + O + O_2 => 2 \ O_2 + O \qquad\qquad k = 1. \ 10^{-38} \ cm^{-3}$$

with rates for these 3-body quenching reactions taken from Vasiljeva et al [13]. For the high pressures of interest here, these quenching reactions are important and represent the most important loss processes for the $O_2(^1\Delta)$. In fact, it is the second of these two quenching reactions which limits the useful upper limit of oxygen partial pressure, as we saw above. Note that the uncertainty in these rate coefficients is a major uncertainty in the calculation of the $O_2(^1\Delta)$ yields.

Gas flow rate has been shown to be an important parameter in the experiments. In order to retain the simplicity of a 2-dimensional model and yet include the finite residence time of the

molecules in the reactor volume due to gas flow, we have simply added a convective flow velocity in the axial direction to all species. Gas is injected from the MHCD side of the computational volume and it is allowed to flow out through a "transparent" anode A2. We have chosen a flow velocity such that the residence time is between 0.1 and 1 ms. A simple estimate assuming a homogeneous flow in the experimental reactor with a flow rate of 250 sccm yields a residence time of about 0.5 ms. As mentioned above, the reality is not so simple – the gas flow is not homogeneous in the reactor because of the complicated geometry and we do not know the residence time in the experimental reactor.

The exact conditions used in out calculations are given in Table I. Each calculations takes several days of computing time on a standard PC.

Gas pressure	30 – 50 torr
Gas mixture	90/10 (Ar/O_2)
Distance between MHCD and 3rd electrode A2	5 mm
Diameter of the MHCD hole	200 μm
Current from the MHCD	1 - 4 mA
Residence time (due to gas flow)	1 ms or 0.1 ms

Table 1: Parameters used in the model calculations.
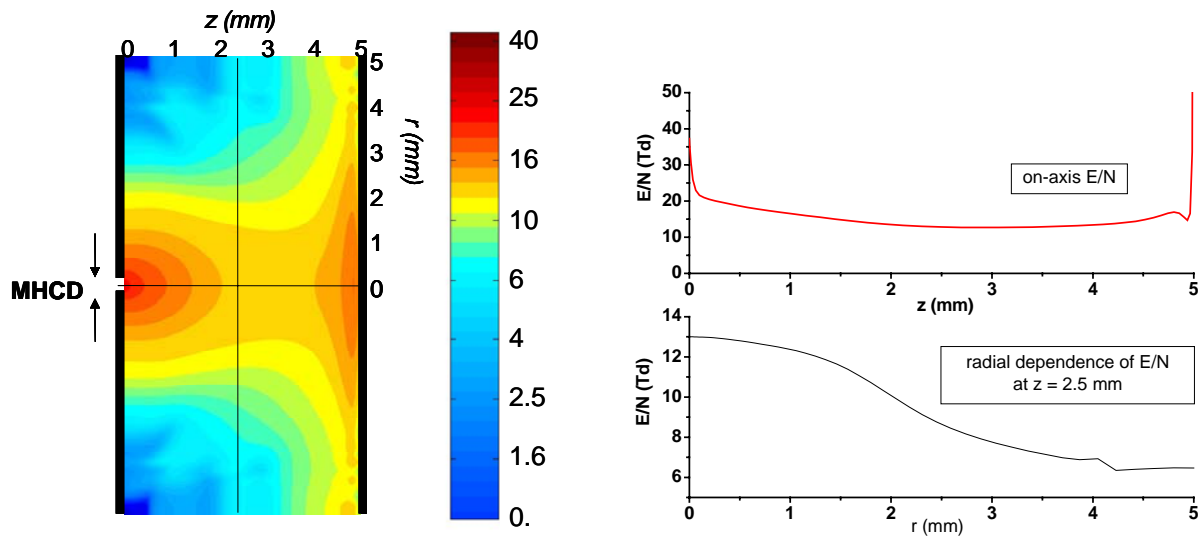
Fig. IX-2 Left : Spatial distribution of reduced electric field E/N calculated for the conditions given in Table 1 with 50 torr, 4 mA and 1 ms residence time.
The color bar gives the scale of E/N in units of Td. Right : axial and radial cuts along the perpendicular lines as indicated in the figure on the left.

The left panel in Fig. IX-2 shows the calculated electric field distribution for 4 mA, and the curves on the right show the axial and radial distributions (at the mid-point). A source of current (the MHCD) is assumed as a boundary condition on the left near the axis as indicated

in fig. IX-1. The electric field – the combination of the geometric field and the space charge field – adjusts itself so as to assure current continuity, with the current collected by anode A2 (the electrode on the right) being the sum of the electron current from the MHCD and any electron current emitted from the surface of A1 due to ion impact. (This is an insignificant component for the conditions here.)   The first feature to note is that the contours of constant E/N resemble closely the visual images of the plasma in the MCS region. E/N determines the mean electron energy and it reflects the plasma conductivity. Thus, we expect the emission from the plasma to depend locally on E/N.   The diameter of the conducting channel increases rapidly near the exit of the MHCD, more slowly near the mid-plane and then there is a radially extended region of high field near the anode A2. This is consistent with all experimental observations.

Let us also mention that parametric studies of the MCSD plasma in argon show that the diameter of the current conducting channel at the mid-plane decreases with increasing current or with increasing pressure. This is also consistent with the trends observed in oxygen containing mixtures as discussed about in Section III.

Low values of E/N favor excitation of $O_2(^1\Delta)$, and in pure oxygen, the optimum value of E/N is about 10 Td. Curves were shown in fig. 19 of our December report showing the influence of admixture of argon and helium on the value of the optimum field. The on-axis field in fig. IX-2 is low, but the optimum value of the field for excitation of $O_2(^1\Delta)$ is predicted to be even lower – at about 3 – 4 Td for argon/oxygen with 10% oxygen. At this low value of E/N, 70% of the energy input to the electrons goes to either $O_2(^1\Delta)$ or $O_2(^1\Sigma)$ which then quenches mainly to the $O_2(^1\Delta)$ level.   At 15 Td in the same 10% mixture, only about 20% of the electrical energy input goes into excitation of $O_2(^1\Delta)$ and $O_2(^1\Sigma)$.   A detailed look at the sources of $O_2(^1\Delta)$ integrated over the computational volume reveals that about 65% of the production of $O_2(^1\Delta)$ is due to direct electron impact excitation. Other contributions to the generation of $O_2(^1\Delta)$ are quenching from $O_2(^1\Sigma)$ and from recombination of O atoms into the $O_2(^1\Sigma)$ state or indirectly from recombination of O atoms into the $O_2(^1\Sigma)$ state.   The conclusion from these numbers is that there is considerable room for further optimization if we can lower the field even further.
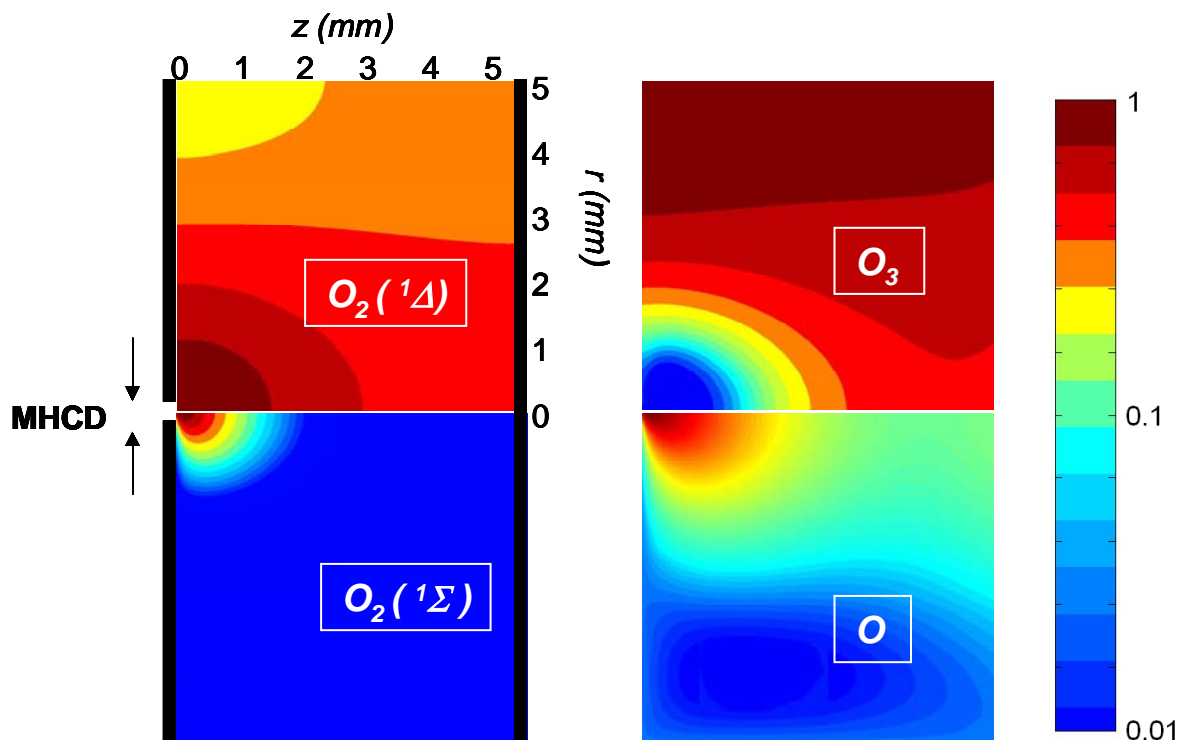
Fig. IX-3. Spatial distributions of principal species in the plasma for same conditions as in fig. IX-2. All species are shown for two orders of magnitude on a log scale (color bar on right) and the relative peak values are as follows : [$O_2(^1\Delta)$] – 3.1 10^{16} cm^{-3} , [$O_2(^1\Sigma)$] – 2.4 10^{16} cm^{-3}; [O_3] – 5.0 10^{15} cm^{-3}, [O] – 8.5 10^{16} cm^-3.

Spatial distributions of the principal excited state species in the plasma are shown in fig. IX-3 for the same conditions as in fig. IX-2; 4 mA, 50 torr and 1 ms residence time of the gas in the computational volume. Comments concerning comparison with experiment are given in Table IX-2.

Fig. IX-4   Calculated spatial distributions of [$O_2(^1\Delta)$] for different operating conditions as indicated. Each panel shows the number density over two order of magnitude range, normalized to the peak number density for each set of conditions.
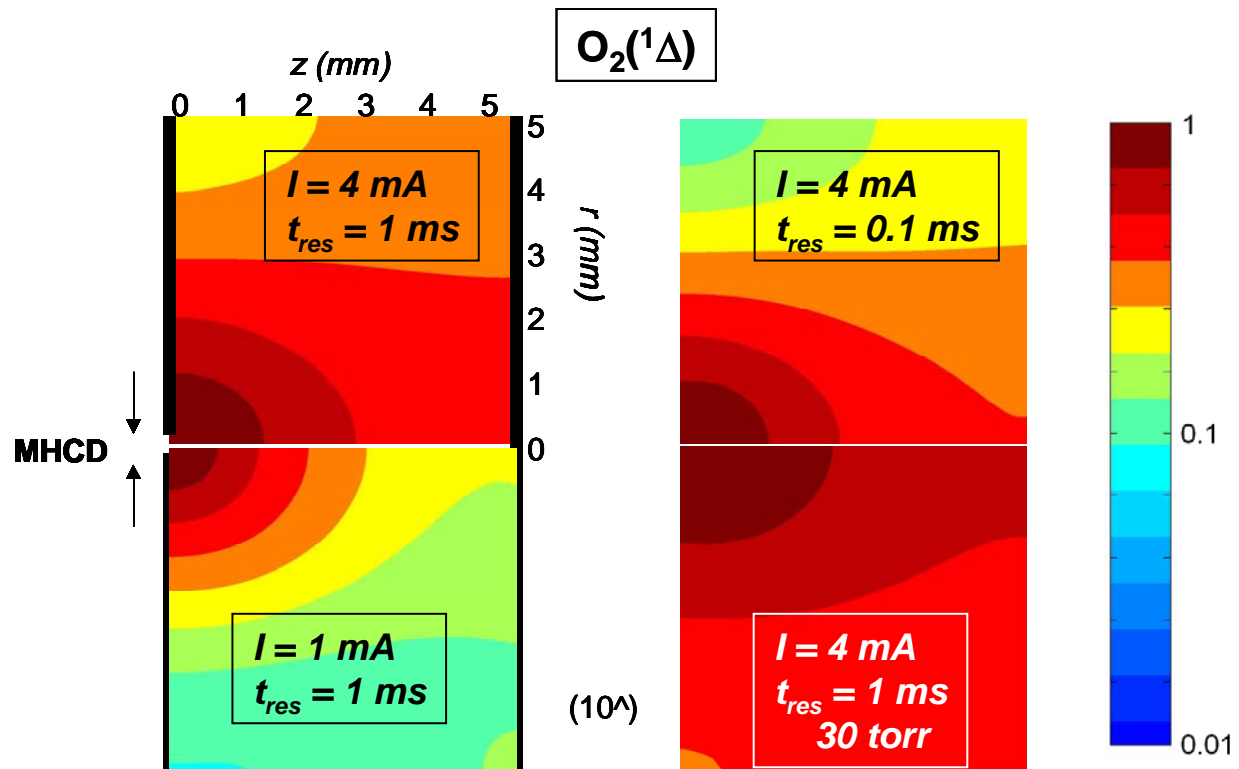*The peaks densities are as follows :*
   4mA, t_{res} = 1 ms , $3.1\,10^{16}\,cm^{-3}$
   4mA, t_{res} = 0.1 ms , $3\,10^{16}\,cm^{-3}$
   1mA, t_{res} = 1 ms , $2\,10^{16}\,cm^{-3}$
   4mA, t_{res} = 1 ms, 30 torr , $1.8\,10^{16}\,cm^{-3}$.
All except the lower right panel are calculated for 50 torr, and the gas mixture is Ar/O_2 with 10% O_2.

The steady-state spatial distributions of the $O_2(^1\Delta)$ are shown in fig. IX-4 for 4 different sets of discharge operating conditions. The baseline case is shown in the top left. Increasing the flow rate – or decreasing the residence time of the gas in the computational volume – has little effect for the conditions here. Decreasing the current leads to a decrease in the $O_2(^1\Delta)$ concentrations, as does a decrease in the total gas pressure. These trends are consistent with experimental observations.

Comparisons with experiment

We wish to emphasize again that the results here are our first results and that much work remains to be done to validate the kinetic scheme, as well as general checking and cross-checking of both experimental and numerical results. Nevertheless, it is worth trying to make some preliminary qualitative comparisons with experiment at this point. These are summarized in Table IX-2.

Experiment	Model	Comments

Visual observation of the plasma in the MCSD region (Section III)	Contours of constant E/N resemble closely the visual images of the plasma in the MCS region.	In all cases, there is bright zone of plasma near the exit of the MHCD. The plasma expands radially from the exit of the MHCD up to a certain point beyond which the diameter of the plasma column is approximately constant. There is a further radial expansion of the luminous region immediately in front of the surface of anode A2, which is almost entirely covered by a luminous layer.
E/N in the plasma is inferred to be between 14 and 21 Td for the conditions studied (Section II)	E/N from the model is about 15 Td.	This good agreement suggests that the electron number balance is reasonably well predicted in the model. The current is essentially an electron current and the current density at a given position is proportional to the local electric field and the electron density
Negative current voltage characteristic for 70 torr, 6% O_2, up to 2 mA (Section II)	Fairly constant voltage between 3 and 4 mA Slightly increasing voltage at 1 mA.	The model calculates the plasma potential distribution in the reactor volume and more work is needed to confirm that this can be compared directly with the measured voltage drop in the MCSD.
Noticeable dependence of electrical properties on gas flow rate (Sections II, III and VII)	No observed dependence on gas flow rate.	The gas flow in the model is parallel to the discharge axis and perpendicular in the experiments. More work is needed to determine how best to compare results.
[O] : localized on axis. Measurements in pure oxygen. (Section VI)	[O] : localized on axis. Calculations in pure in Ar/O_2.	The same trend is observed - localization of [O] on the discharge axis and slow decrease with axial position. However, the conditions of the calculations are too different to draw more precise conclusions yet.
[O_3] : observed to be fairly homogeneous in the reactor volume (Section V)	[O_3] : predicted to vary less than a factor of 2 radially in the reactor.	The absolute value predicted by the model at 1 mA is 5 times larger than measured in the experiment at 1 mA. This is considered to be acceptable agreement at this stage.
$O_2(^1\Delta)$ density is measured downstream from the reactor and depends on gas flow rate. (Section VII)	$O_2(^1\Delta)$ predicted in the MCSD volume. Predicted to increase with discharge current and decrease with increasing gas flow rate.	Agreement in the magnitude of the $O_2(^1\Delta)$ density is good at this point. The model predicts a volume average density consistent with measured values on the same order and dependencies on current and gas flow.

Table IX-2. Qualitative comparison model/experiment in Ar/O_2 mixtures.

51

X. Conclusions

We have successfully demonstrated that copious quantities of $O_2(^1\Delta)$ are generated in oxygen containing mixtures in microcathode sustained discharges (MCSDs). The high-pressure and low-temperature plasma conditions in the MCSD region make these sources potential very interesting for e-COIL and other applications where high yields of $O_2(^1\Delta)$ are desired.

Highlights from our work during this reporting period are listed in the summary at the beginning of the report.

Our main effort during this phase of our contract has been to characterize the plasma in the MCSD volume, with particular emphasis in the measurement of the $O_2(^1\Delta)$ number densities. To this end we have estimated the electric field in this region, measured the gas temperature, and we have made absolute measurements of the number densities of atomic oxygen, ozone, and the $O_2(^1\Delta)$. Measurements of the $O_2(^1\Delta)$ proved to be particularly challenging. The calorimeter system we constructed to make these measurements has consistently yielded null results, for reasons we do not understand. Emission spectroscopy was therefore the only diagnostic we had to measure the $O_2(^1\Delta)$ number densities.

A predictive model has been developed and this is just beginning to yield interesting results. More work is needed for validation and comparisons with experiment are underway. We expect that the model will be a very useful tool to help understand the plasma in the MCSD and to help guide experimental optimization of these discharges.

Our results are still preliminary. More work is needed to understand the result and to move forward towards developing systems that optimize the yield. Further work should proceed along the following lines :
- confirmation of the experimental results for $O_2(^1\Delta)$ number densities using other diagnostic techniques
- evaluation of limits of stability and limits of control of E/N in the MCSD region
- experimental optimization of the yield using as parameters : gas pressure, flow, mixture, current, MHCD geometry
- scale up to multiple discharges
- exploration of alternate discharge geometries
- pulsed discharges.

We hope to have the opportunity to continue in these very interesting directions.

References

1. Final report EOARD Grant F18655-05-1-3039, December 2005, "Microdischarge sources of $O_2(^1\Delta)$", prepared by L.C. Pitchford.

2. K.H. Schoenbach, A. El-Habachi, W. Shi, and M. Ciocca, Plasma Sources Sci. Technol. **6** 468 (1997); K.H. Schoenbach, A. El-Habachi, M.M. Moselhy, W. Shi, and R.H. Stark, Phys. Plasmas **7** 286 (2000).

3. R.H. Stark and K.H. Schoenbach, J. Appl. Phys. **85** 2075 (1999); R.H. Stark and K.H. Schoenbach, J. Appl. Phys. **89** 3568 (2001); Abdel-Aleam H. Mohamed, Rolf Block, and Karl H. Schoenbach, IEEE Trans Plasma Sci, **30** (2002).

4. A. Rousseau and X. Aubert J. Phys.D : Appl. Phys. **39** 1619 (2006); X. Aubert, et al, "Analysis of the self-pulsing operating mode of a microdischarge" submitted to Plasma Sources Sci. and Technol. (2006).

5. M Touzeau, M Vialle, A Zellagui, G Gousset, M Lefebvre and M Pealat, J. Phys D: Appl. Phys. **24** 41 (1991).

6. M Miclea, K Kunze, U Heitmann, S Florek, J Franzke and K Niemax, J. Phys. D: Appl. Phys. **38** 1709 (2005).

7. Frank Leipold, Robert H Stark, Ahmed El-Habachi and Karl H Schoenbach, J. Phys. D: Appl. Phys. **33** 2268 (2000).

8. B. Eliasson, M. Hirth, and U. Kogelschatz, J. Phys. D: Appl. Phys. **20** 1421 (1987).

9. Molina et al, J. Geophys. Res. **91**, D13 (1986).

10. H F Döbele et al, Plasma Sources Sci. Technol. **14** s31-s41 (2005).

11 Newman S M, Orr-Ewing A J, Newnham D A and Ballard J J. Phys. Chem. **A 104** 9467 (2000).

12. D.S Stafford.and M.J Kushner, J. App. Phys. **96** 2451 (2004).

13. A.N. Vasiljeva, K.S. Klopovskiy, et al, J. Phys.D: Appl. Phys. **37** 2455 (2004) .